Table 1. Nucleotide Diversity and Summary Statistics.

Region	Pop.[a]	S[b]	θ_w ($\times 10^{-4}$)		π ($\times 10^{-4}$)		Tajima's D Statistic			Fu and Li's D*			Fu and Li's F*		
			Rank		Rank		Rank		P	Rank		P	Rank		P
$RAC2_{iS}$ (4,202 bp)	YRI	21	11.75	0.78	13.89	0.93	0.61	0.90	0.085	0.021	0.66	0.38	0.26	0.75	0.24
	CEU	14	7.83	0.78	11.00	0.87	1.28	0.87	0.079	−0.28	0.47	0.41	0.27	0.62	0.37
	AS	14	7.83	0.82	10.01	0.86	0.88	0.77	0.22	0.17	0.65	0.43	0.47	0.70	0.34
$RAC2_{3'}$ (5,560 bp)	YRI	53	22.38	0.99	27.41	0.99	0.80	0.95	0.032	0.72	0.90	0.052	0.89	0.94	0.028
	CEU	42	17.74	0.98	23.51	0.99	1.15	0.83	0.11	0.95	0.85	0.10	1.21	0.90	0.073
	AS	39	16.47	0.99	15.84	0.95	−0.14	0.47	0.39	1.66	>0.99	0.0038	1.23	0.91	0.086

[a] Population.
[b] Number of segregating sites.

neutrality was observed for $RAC2_{inS}$ (table 1). Coalescent simulations using different demographic models (Marth et al. 2004; Voight et al. 2005) yielded very similar results and are available as supplementary table S2, Supplementary Material online.

In order to further explore the possibility that nucleotide diversity at the $RAC2_{3'}$ region has been maintained by selection, we applied an MLHKA by comparing polymorphisms and divergence levels at $RAC2_{inS}$ and $RAC2_{3'}$ with 16 NIEHS genes resequenced in the three populations we analyzed (see Materials and Methods). Under neutral evolution, the amount of within-species diversity is predicted to correlate with levels of between-species divergence since both depend on the neutral mutation rate (Kimura 1983). The MLHKA test (Wright and Charlesworth 2004) is commonly used to verify this expectation. Results are shown in table 2 and indicate that for $RAC2_{3'}$, a significant excess of polymorphisms compared with divergence is observed in all populations. Conversely, no deviations from neutral expectations was observed for the $RAC2_{inS}$ region (with only borderline significance in YRI).

Under a balancing selection regime, polymorphisms may be maintained in populations for a time, which is longer than expected under neutrality. We used GENETREE to estimate the TMRCA of the $RAC2_{3'}$ haplotype genealogy. The method is based on a maximum likelihood coalescent analysis (Griffiths and Tavare 1994, 1995) and assumes an infinite-site model without recombination. Therefore, haplotypes and sites that violate these assumptions need to be removed. Given the relatively low recombination rate in the region, only nine single segregating sites had to be removed. The resulting gene tree, rooted using the chimpanzee sequence, is partitioned into two deep clades, with clade A further divided into two minor branches (fig. 2) (clades A1 and A2). Using this method, the TMRCA of the whole genealogy amounted to 2.54 My (standard deviation: 0.374 My), whereas the two subclades (A1 and A2) have a shallower TMRCA of around 1.1 My.

Table 2. MLHKA Test.

Region	Fixed Sub[a]	MLHKA YRI k[b]	YRI P	CEU k[b]	CEU P	AS k[b]	AS P
$RAC2_{inS}$	30	2.35	0.048	2.24	0.13	2.25	0.89
$RAC2_{3'}$	59	3.24	2.6×10^{-3}	3.72	4.0×10^{-4}	3.50	8.6×10^{-4}

[a] Number of fixed substitutions (human/chimpanzee).
[b] Selection parameter ($k > 1$ indicates an excess of polymorphism relative to divergence).

Haplotype Analysis and Association with Autoimmune Diseases

In order to gain insight into the distribution of *RAC2* haplotypes in human populations, we constructed a median-joining network (Bandelt et al. 1999) using all variants identified in $RAC2_{inS}$ and $RAC2_{3'}$ with the exclusion of singletons (fig. 3). The topology largely recapitulates the one obtained using GENETREE with two major clades (A and B), and haplotypes in clade A subdivided into two further haplogroups (referred to as A1 and A2) (fig. 3). There are clear differences in the distribution of *RAC2* haplotypes among the three populations we analyzed, although F_{st} values (Wright 1950) were not exceptional compared with those calculated for 5 kb reference windows (supplementary table S3, Supplementary Material online). Estimates of allelic richness (and private allelic richness) within haplogroups were calculated using a rarefaction procedure (Kalinowski 2004) to account for different haplogroup frequency; results indicated that haplogroup A2 had the lowest genetic diversity among the three haplotype clades, whereas B haplotype tended to have high allelic richness (supplementary table S4, Supplementary Material online).

The pivotal role of *RAC2* in immune response led us to verify whether the three major haplogroups were differentially represented when healthy controls were compared with subjects suffering from autoimmune diseases such as MS and CD, two diseases with a strong genetic basis (Weng et al. 2007; Nielsen et al. 2008; Langer-Gould et al. 2010) that suggests the presence of shared genetic determinants.

We selected two variants: rs2899284, located along the major branch separating clades A and B, and rs739041 that identifies haplogroup A1 (fig. 3). The typing of these two variants allows unequivocal haplogroup inference in European populations, as they are nonrecurrent in the phylogeny. The allele frequency of rs2899284 (T) and rs739041 (C) in the three populations we analyzed were as follows: CEU, 0.22 and 0.45; YRI, 0.27 and 0.67; and AS, 0.10 and 0.30.

The two SNPs were genotyped in 387 patients with RRMS and in 149 subjects suffering from CD; two independent cohorts of sex- and aged-matched controls were also

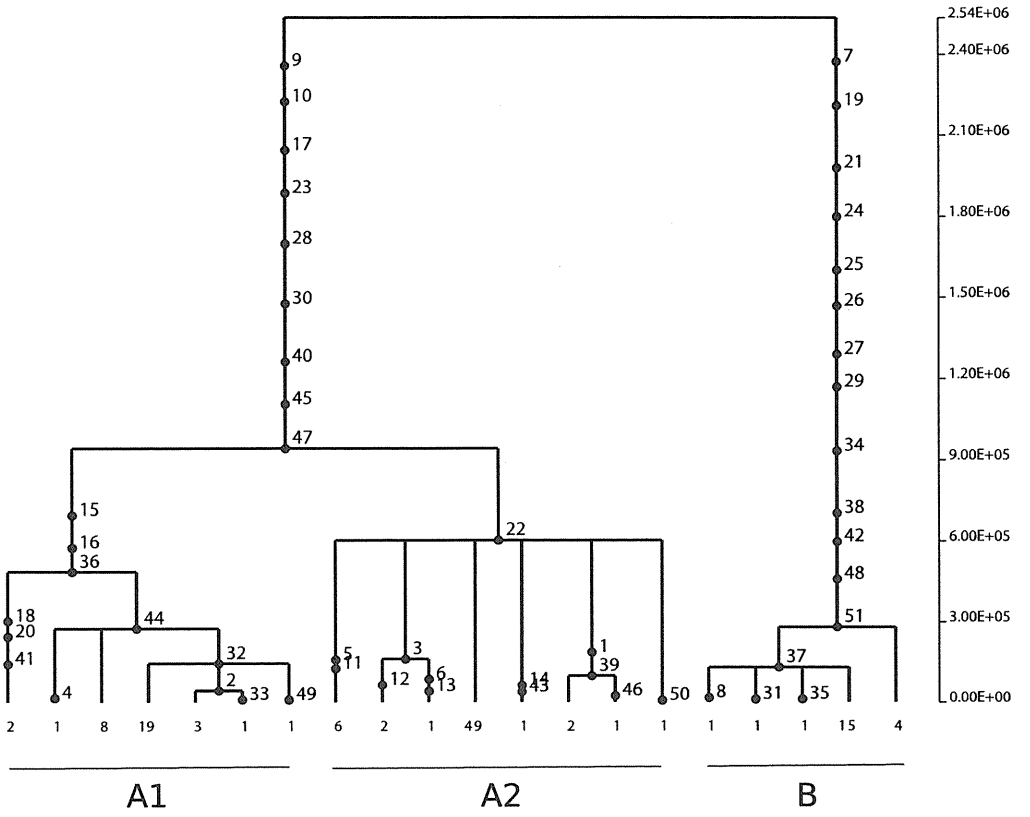

FIG. 2. Estimated haplotype tree for the *RAC2*$_3$' gene region. Mutations are represented as black dots and named for their physical position along the regions. The absolute frequency of each haplotype is reported.

analyzed. Using logistic regression analysis, haplotypes belonging to haplogroup B resulted to be significantly associated to disease status in both the RRMS and CD case/control studies (table 3).

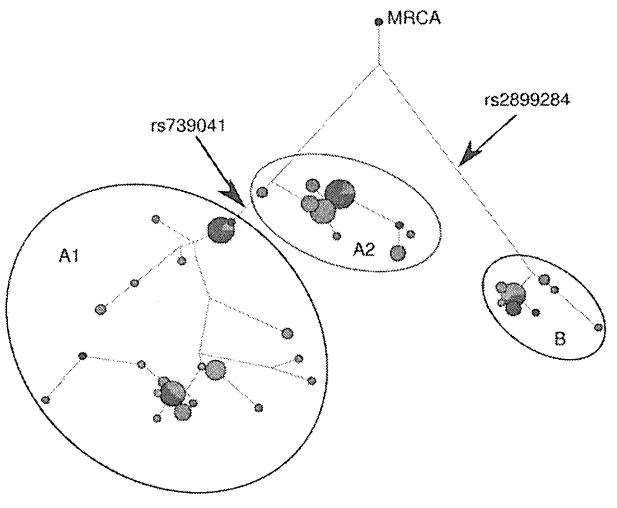

FIG. 3. Median-joining network of *RAC2* haplotypes. Each node represents a different haplotype, with the size of the circle proportional to frequency. Branch lengths are proportional to the number of nucleotide differences. Circles are color coded according to population (green: YRI, blue: CEU, and red: AS). The most recent common ancestor (MRCA) also shown (black circle). The three major haplogroups are evidenced, as well as the position of the two SNPs genotypes in patients and controls.

Although we did not expect substantial levels of population structure in our cohorts as all subjects were Italians with Caucasian ancestry, we verified that the results we obtained are not secondary to cryptic substructure. To this aim, we genotyped RRMS subjects and controls for 15 null SNPs (see Materials and Methods). This procedure was not performed for CD patients as additional genetic material was unavailable. We used null SNPs to apply the GC method (Devlin et al. 2001): Calculation of the inflation parameter λ resulted in a value of 0.92, suggesting that there is no substantial stratification in our samples. Yet, the GC method may not be conservative when few markers are used (Balding 2006). Thus, we used the program STRUCTURE 2.1 (Pritchard et al. 2000; Falush et al. 2003) and included the inferred ancestry proportions of individual cases and controls as continuous covariates in the logistic regression analysis. A significant result was again obtained for haplotypes belonging to haplogroup B.

We next verified whether *RAC2* haplotypes also affected disease expression in RRMS and CD by testing for correlations between haplotypes and age at disease onset. This latter information was available for 325 and 147 RRMS and CD patients, respectively. As shown in table 4, no association was observed between age at onset in CD and *RAC2* haplotypes. Conversely, in the case of MS, haplotypes in group B were associated with a significantly earlier presentation of symptoms, whereas the opposite was observed for haplotypes in cluster A2 (table 4). The same results were obtained after accounting for the presence of the

Table 3. Association of *RAC2* Haplotypes with Susceptibility to RRMS and CD.

Haplogroup	Frequency		OR (95% CI)	P	OR (95% CI)[a]	P[a]
	RRMS (n = 387)	Controls (n = 335)				
A1	0.270	0.289	0.91 (0.71–1.13)	0.426	0.91 (0.71–1.14)	0.416
A2	0.390	0.424	0.85 (0.69–1.07)	0.166	0.85 (0.68–1.07)	0.161
B	0.340	287	1.30 (1.04–1.64)	0.024	1.31 (1.05–1.66)	0.022
	CD (n = 149)	Controls (n = 164)				
A1	0.267	0.287	0.90 (0.64–1.30)	0.556	NP	NP
A2	384	0.439	0.78 (0.58–1.09)	0.136	NP	NP
B	0.349	0.274	1.41 (1.01–1.99)	0.048	NP	NP

NOTE.—CI, confidence interval; NP, not performed; OR, odds ratio.
[a] Adjusted for admixture.

*HLA-DRB*15* allele, a known risk factor for RRMS in Caucasians (supplementary table S5, Supplementary Material online).

Discussion

RAC2 is a protein expressed in the hematopoietic cell lineage and is involved in signal transduction in various cellular processes, such as chemotaxis, cytoskeletal rearrangement, cellular differentiation, and proliferation (Heasman and Ridley 2008). Production of proinflammatory cytokines and cysteine cysteine (CC) chemokines, secretion of reactive oxygen species by neutrophils, and cyclooxygenase-2 (COX-2) production by macrophages are also modulated by RAC2 (Heasman and Ridley 2008). Thus, RAC2 is a key player in the inflammation process, acting at different levels, and being involved in multiple mechanisms of immunity.

The state of *RAC2* expression influences the ability of this gene to trigger inflammatory responses. Some pathogens, in fact, downregulate *RAC2* transcription to escape cellular innate immune response (i.e., respiratory burst activation), facilitating their intracellular survival (Carlyon et al. 2002). Similarly, both bacterial and viral pathogens were shown to have the ability to target the protein product of *RAC2* and alter its activity (Janardhan et al. 2004; Chung et al. 2010; Groves et al. 2010). Among these pathogens, the SIV- and HIV-encoded Nef proteins interact with RAC2 to alter T-cell function (Janardhan et al. 2004). Notably, recent data indicate a significant association between chromosome microsatellite markers in 22q12-13 (where RAC2 is located) and resistance to HIV infection in HIV exposed but uninfected individuals (Kanari et al. 2005). An accurate analysis of this region allowed the identification of *RAC2* gene SNPs that were significantly associated with the resistance phenotype displayed by exposed uninfected individuals and with the development of particularly potent HIV-specific cell-mediated immunity (Kanary Y, Hakata Y, et al. 2012).

Table 4. Association of *RAC2* Haplotypes with Age at Onset in RRMS and IBD.

Disease	Haplogroup	BETA	P
RRMS (n = 325)	A1	0.382	0.602
	A2	1.551	0.029
	B	−1.519	0.025
CD (n = 147)	A1	−0.137	0.940
	A2	−1.558	0.349
	B	1.578	0.326

NOTE.—BETA is the regression coefficient.

In general, these observations indicate that RAC2 may be involved in host–pathogen genetic conflicts; consequently, the gene may represent a target of natural selection and harbor variants that affect the susceptibility to infectious diseases or other immunological phenotypes in humans. Nonetheless, inspection of available databases revealed no polymorphic amino acid variation segregating at detectable frequency in human populations, suggesting that functional polymorphisms in *RAC2*, if present, may occur within regulatory noncoding regions. We therefore exploited interspecific genetic diversity data to identify gene regions that may harbor functional noncoding sequences and analyzed their evolutionary pattern in three human populations. Our data indicate that the genomic portion covering the 3′ gene region displays extremely high nucleotide diversity, an excess of intermediate frequency alleles, and a higher level of within-species diversity compared with interspecific divergence, as assessed by the MLHKA test.

All these features strongly suggest the action of balancing selection. In particular, analysis of haplotype genealogy indicated the presence of three clades, which is consistent with a model of multiallelic balancing selection. This observation is in line with values of SFS-based statistics (Tajima's *D* and Fu and Li's *F** and *D** statistics), which are not strikingly positive, as the skew towards intermediate frequency variants tends to be less marked in a multiallelic selection model than in the case of biallelic selection. Calculation of the TMRCA for the $RAC2_{3'}$ haplotype genealogy yielded and estimate of 2.54 My, a coalescence time deeper than those estimated for most neutrally evolving autosomal human loci, which range from 0.8 to 1.5 My (Garrigan and Hammer 2006). Overall, these data strongly suggest that long-term balancing selection has maintained distinct functional alleles in *RAC2*. Inspection of polymorphisms located along the major branches of the genealogy indicated that several variants in DNaseI hypersensitive sites divide clade A and B haplotypes. In particular, variants rs933222, rs933221, rs4821610, and rs4821609 occur within a 600 bp portion located downstream the transcription end site; this region displays histone marks associated with enhancers (H3K4Me1 and H3K27Ac) in lymphoblastoid cell lines, suggesting that one or a combination of these SNPs alter RAC2 transcriptional activity and represent

functional variants. Experimental analyses will be required to evaluate this possibility. Similarly, rs9798725 (immediately downstream the transcription end site) occurs within a sequence conserved in mammals and separates the two major clades of the phylogeny.

It is worth mentioning that evolutionary scenarios different from balancing selection might account for the results we obtained. One alternative possibility is that the high nucleotide diversity we observed at the $RAC2_{3'}$ gene region is the result of a relaxation of selective constraint (which allows accumulation of new mutations). Yet, the region was selected because of the presence of DNaseI hypersensitive sites and sequence elements conserved across mammals and primates. Thus, relaxation of functional constraints would have occurred recently, with the only involvement of human populations. Moreover, nucleotide diversity in the region is extremely high, ranking above the 98th percentile in the distribution of reference windows. These latter are randomly drawn from resequenced genes and most of them cover intronic regions, where functional constraints are expected to be relatively relaxed; thus, we believe that the high diversity at $RAC2_{3'}$ is more likely to result from a selective process. Indeed, an alternative explanation to balancing selection is diversifying selection, which refers to a situation whereby genotypes are favored merely because they are different and therefore results in the maintenance of multiple alleles. This is an interesting possibility that might fit the evolutionary history of a gene involved in immune response that, as mentioned above, is targeted by different pathogen species. Yet, the molecular signatures of balancing and diversifying selection are difficult to disentangle, and population genetics analyses only provide a snapshot of a dynamic evolutionary process, making it difficult to precisely determine the underlying selective regime. For example, although F_{ST} was not exceptionally high, clear differences can be appreciated in the distribution of *RAC2* haplotypes across ethnic groups, suggesting that locally exerted selective pressures might have been acting during a more recent time frame.

From a biological perspective, one possibility is that the three major *RAC2* haplotypes are differentially active in distinct cell types or modulate gene expression in response to diverse stimuli. A similar hypothesis has been proposed to explain long-term balancing selection in the promoter region of major histocompatibility complex class II genes (Cowell et al. 1998; Beaty et al. 1999; Loisel et al. 2006). This view is consistent with the recent demonstration (Dimas et al. 2009) that the majority of variants affecting gene regulation in the human genome are cell-type specific, and that cell-specific regulatory elements tend to localize relatively distant from the transcription start site. An alternative possibility is that distinct alleles may have been selected to prevent the down-modulation or misregulation of *RAC2* transcription exerted by pathogens (Carlyon et al. 2002). Under these scenarios, the selective pressure acting on RAC2 is expected to be pathogen driven. Yet, other authors (Ferrer-Admetlla et al. 2008) have recently suggested that the maintenance of genetic diversity at immune response loci may result from the need to balance protection against invading pathogens with maintenance of self-tolerance. Indeed, our data indicate that haplotypes in *RAC2* associate with predisposition to MS and CD. Specifically, haplotypes belonging to clade B were significantly more common in patients compared with controls, and in RRMS patients, the presence of B haplotypes correlated with an earlier presentation of disease symptoms. Growing evidences in recent years have indicated that a portion of susceptibility alleles is shared among two or more autoimmune conditions (reviewed in Zenewicz et al. 2010). This observation has been interpreted in terms of common disease pathways being involved in the pathogenesis of autoimmune disorders and partially explains the cooccurrence of distinct autoimmune conditions in patients and families. Indeed, several studies have indicated that some degree of comorbidity is observed between MS and CD in affected individuals and their family members (Weng et al. 2007; Nielsen et al. 2008; Langer-Gould et al. 2010). Therefore, our association of the same haplotype with susceptibility to both MS and CD can be regarded as a strong confirmation of the causal role of RAC2 variants in the pathogenesis of autoimmune diseases.

As mentioned above, RAC2 is thought to have a central role in the regulation of RICD, a mechanism that contributes to the maintenance of CD4+ T-cell tolerance. Physiologically, RICD occurs more often with self rather that foreign antigens and is therefore considered as a "propriocidal" form of cell death that limits T-cell expansion in the presence of persistent antigen (reviewed in Snow et al. 2010). In this light, gene products involved in RICD can be regarded as excellent candidates to carry variants associated with autoimmune diseases. Indeed, polymorphisms in Fas and FasL have previously been associated with susceptibility to MS (Zayas et al. 2001; van Veen et al. 2002; Kantarci et al. 2004; Lucas et al. 2004), and a recent genome-wide association study for primary sclerosing cholangitis (Melum et al. 2011), an autoimmune conditions that often occurs in IBD patients, identified an SNP close to the *BCL2L11* gene (also known as BIM), another key player in the elicitation of RICD (Snow et al. 2010). Therefore, our data are in agreement with the conundrum whereby distinct susceptibility variants for a given trait may occur in genes that participate in a shared molecular pathway.

Despite the fact that our data indicate *RAC2* as a susceptibility gene for autoimmune diseases, it remains to be evaluated whether the predisposition to autoimmunity can be regarded as a selective pressure during the evolutionary history of humans. In fact, Plenge (2010) reported that the prevalence of several autoimmune disorders, including MS, is increasing in human communities (at least in developed countries) but their contribution to population fitness throughout human history, although unknown, can hardly be regarded as comparable to that of infectious diseases. Therefore, we tend to favor a model whereby balancing selection in the *RAC2* regulatory 3′ gene region is pathogen driven, and the resulting maintenance of susceptibility alleles for CD and MS can be regarded as a by-product of long-term

selection (reviewed in Sironi and Clerici 2010). Indeed, pathogen-driven balancing selection has previously been shown to maintain a subset of susceptibility alleles for IBD in human populations (Fumagalli, Pozzali, et al. 2009).

In summary, data herein show that integration of different approaches can provide valuable insight into the location of putative functional variants and on haplotype structure, which in turn can be applied to association studies. We describe for the first time an association between specific haplotypes of the *RAC2* gene and autoimmunity. Therapeutic approaches aimed at inhibiting or, at least, decreasing *RAC2* expression and/or activity could be beneficial in these patients. Statins were shown to interfere with RAC2 activity, limiting both T-cell activation and COX-2 macrophages production (Brinkkoetter et al. 2006; Habib et al. 2007). Notably, recent results indicated that atorvastatin, a statin, has beneficial antiinflammatory effects in CD patients (Grip et al. 2008).

Therefore, these results, although needing validation in bigger cohorts, suggest that RAC2 plays a potentially important role in the immunopathogenesis of autoimmune disease, possibly as a consequence of the ability of this gene to regulate T lymphocytes activity. Modulation of *RAC2* activity might be a novel potential therapeutic target in patients with autoimmune diseases.

Supplementary Material

Supplementary tables 1–5 are available at *Molecular Biology and Evolution* online (http://www.mbe.oxfordjournals.org/).

Acknowledgments

M.C. is supported by grants from The Eli and Edythe Broad Foundation (IBD-0294), Istituto Superiore di Sanita' "Programma Nazionale di Ricerca sull' AIDS", the EMPRO and AVIP EC WP6 Projects, the nGIN EC WP7 Project, the Japan Health Science Foundation, 2008 Ricerca Finalizzata (Italian Ministry of Health), 2008 Ricerca Corrente (Italian Ministry of Health), Progetto FIRB RETI: Rete Italiana Chimica Farmaceutica CHEM-PROFARMA-NET (RBPR05NWWC), and Fondazione CARIPLO.

References

Asthana S, Schmidt S, Sunyaev S. 2005. A limited role for balancing selection. *Trends Genet.* 21:30–32.

Balding DJ. 2006. A tutorial on statistical methods for population association studies. *Nat Rev Genet.* 7:781–791.

Bandelt HJ, Forster P, Rohl A. 1999. Median-joining networks for inferring intraspecific phylogenies. *Mol Biol Evol.* 16:37–48.

Barreiro LB, Quintana-Murci L. 2010. From evolutionary genetics to human immunology: how selection shapes host defence genes. *Nat Rev Genet.* 11:17–30.

Beaty JS, Sukiennicki TL, Nepom GT. 1999. Allelic variation in transcription modulates MHC class II expression and function. *Microbes Infect.* 1:919–927.

Benvenuti F, Hugues S, Walmsley M, Ruf S, Fetler L, Popoff M, Tybulewicz VL, Amigorena S. 2004. Requirement of Rac1 and Rac2 expression by mature dendritic cells for T cell priming. *Science* 305:1150–1153.

Boyle AP, Davis S, Shulha HP, Meltzer P, Margulies EH, Weng Z, Furey TS, Crawford GE. 2008. High-resolution mapping and characterization of open chromatin across the genome. *Cell* 132:311–322.

Brinkkoetter PT, Gottmann U, Schulte J, van der Woude FJ, Braun C, Yard BA. 2006. Atorvastatin interferes with activation of human CD4(+) T cells via inhibition of small guanosine triphosphatase (GTPase) activity and caspase-independent apoptosis. *Clin Exp Immunol.* 146:524–532.

Carlyon JA, Chan WT, Galan J, Roos D, Fikrig E. 2002. Repression of rac2 mRNA expression by anaplasma phagocytophila is essential to the inhibition of superoxide production and bacterial proliferation. *J Immunol.* 169:7009–7018.

Charlesworth D. 2006. Balancing selection and its effects on sequences in nearby genome regions. *PLoS Genet.* 2:e64.

Chung KJ, Cho EJ, Kim MK, et al. (11 co-authors). 2010. RtxA1-induced expression of the small GTPase Rac2 plays a key role in the pathogenicity of Vibrio vulnificus. *J Infect Dis.* 201:97–105.

Cowell LG, Kepler TB, Janitz M, Lauster R, Mitchison NA. 1998. The distribution of variation in regulatory gene segments, as present in MHC class II promoters. *Genome Res.* 8:124–134.

Croker BA, Tarlinton DM, Cluse LA, Tuxen AJ, Light A, Yang FC, Williams DA, Roberts AW. 2002. The Rac2 guanosine triphosphatase regulates B lymphocyte antigen receptor responses and chemotaxis and is required for establishment of B-1a and marginal zone B lymphocytes. *J Immunol.* 168:3376–3386.

Decoursey TE, Ligeti E. 2005. Regulation and termination of NADPH oxidase activity. *Cell Mol Life Sci.* 62:2173–2193.

Devlin B, Roeder K, Bacanu SA. 2001. Unbiased methods for population-based association studies. *Genet Epidemiol.* 21:273–284.

Dimas AS, Deutsch S, Stranger BE, et al. (11 co-authors). 2009. Common regulatory variation impacts gene expression in a cell type-dependent manner. *Science* 325:1246–1250.

Enoch MA, Shen PH, Xu K, Hodgkinson C, Goldman D. 2006. Using ancestry-informative markers to define populations and detect population stratification. *J Psychopharmacol.* 20:19–26.

Evanno G, Regnaut S, Goudet J. 2005. Detecting the number of clusters of individuals using the software STRUCTURE: a simulation study. *Mol Ecol.* 14:2611–2620.

Falush D, Stephens M, Pritchard JK. 2003. Inference of population structure using multilocus genotype data: linked loci and correlated allele frequencies. *Genetics* 164:1567–1587.

Ferrer-Admetlla A, Bosch E, Sikora M, et al. (11 co-authors). 2008. Balancing selection is the main force shaping the evolution of innate immunity genes. *J Immunol.* 181:1315–1322.

Fu YX, Li WH. 1993. Statistical tests of neutrality of mutations. *Genetics* 133:693–709.

Fumagalli M, Cagliani R, Pozzoli U, Riva S, Comi GP, Menozzi G, Bresolin N, Sironi M. 2009. Widespread balancing selection and pathogen-driven selection at blood group antigen genes. *Genome Res.* 19:199–212.

Fumagalli M, Pozzoli U, Cagliani R, Comi GP, Riva S, Clerici M, Bresolin N, Sironi M. 2009. Parasites represent a major selective force for interleukin genes and shape the genetic predisposition to autoimmune conditions. *J Exp Med.* 206:1395–1408.

Garrigan D, Hammer MF. 2006. Reconstructing human origins in the genomic era. *Nat Rev Genet.* 7:669–680.

Glazko GV, Nei M. 2003. Estimation of divergence times for major lineages of primate species. *Mol Biol Evol.* 20:424–434.

Gonzalez JR, Armengol L, Sole X, Guino E, Mercader JM, Estivill X, Moreno V. 2007. SNPassoc: an R package to perform whole genome association studies. *Bioinformatics* 23:644–645.

Griffiths RC, Tavare S. 1994. Sampling theory for neutral alleles in a varying environment. *Philos Trans R Soc Lond B Biol Sci.* 344:403–410.

Griffiths RC, Tavare S. 1995. Unrooted genealogical tree probabilities in the infinitely-many-sites model. *Math Biosci.* 127:77–98.

Grip O, Janciauskiene S, Bredberg A. 2008. Use of atorvastatin as an anti-inflammatory treatment in Crohn's disease. *Br J Pharmacol.* 155:1085–1092.

Groves E, Rittinger K, Amstutz M, Berry S, Holden DW, Cornelis GR, Caron E. 2010. Sequestering of Rac by the Yersinia effector YopO blocks Fcgamma receptor-mediated phagocytosis. *J Biol Chem.* 285:4087–4098.

Habib A, Shamseddeen I, Nasrallah MS, Antoun TA, Nemer G, Bertoglio J, Badreddine R, Badr KF. 2007. Modulation of COX-2 expression by statins in human monocytic cells. *FASEB J.* 21: 1665–1674.

Heasman SJ, Ridley AJ. 2008. Mammalian rho GTPases: new insights into their functions from in vivo studies. *Nat Rev Mol Cell Biol.* 9:690–701.

Hudson RR. 2002. Generating samples under a Wright-Fisher neutral model of genetic variation. *Bioinformatics* 18:337–338.

Hurst LD. 2009. Fundamental concepts in genetics: genetics and the understanding of selection. *Nat Rev Genet.* 10:83–93.

Janardhan A, Swigut T, Hill B, Myers MP, Skowronski J. 2004. HIV-1 Nef binds the DOCK2-ELMO1 complex to activate rac and inhibit lymphocyte chemotaxis. *PLoS Biol.* 2:E6.

Kalinowski ST. 2004. Counting alleles with rarefaction: private alleles and hierarchical sampling designs. *Conserv Genet.* 5:539–543.

Kanari Y, Clerici M, Abe H, et al. (12 co-authors). 2005. Genotypes at chromosome 22q12-13 are associated with HIV-1-exposed but uninfected status in Italians. *AIDS.* 19:1015–1024.

Kanari Y, Hakata Y, Wichukchinda N, et al. (23 co-authors). Forthcoming 2012. High-level *Rac2* expression associated with intron polymorphisms restricts HIV-1 replication in human cells. *J Clin Invest.*

Kantarci OH, Hebrink DD, Achenbach SJ, Atkinson EJ, de Andrade M, McMurray CT, Weinshenker BG. 2004. CD95 polymorphisms are associated with susceptibility to MS in women. A population-based study of CD95 and CD95L in MS. *J Neuroimmunol.* 146:162–170.

Kim C, Dinauer MC. 2001. Rac2 is an essential regulator of neutrophil nicotinamide adenine dinucleotide phosphate oxidase activation in response to specific signaling pathways. *J Immunol.* 166:1223–1232.

Kimura M. 1983. The neutral theory of molecular evolution. Cambridge: Cambridge University Press.

Knaus UG, Heyworth PG, Evans T, Curnutte JT, Bokoch GM. 1991. Regulation of phagocyte oxygen radical production by the GTP-binding protein Rac 2. *Science* 254:1512–1515.

Langer-Gould A, Albers KB, Van Den Eeden SK, Nelson LM. 2010. Autoimmune diseases prior to the diagnosis of multiple sclerosis: a population-based case-control study. *Mult Scler.* 16:855–861.

Lennard-Jones JE. 1989. Classification of inflammatory bowel disease. *Scand J Gastroenterol Suppl.* 170:2–6.

Li B, Yu H, Zheng W, Voll R, Na S, Roberts AW, Williams DA, Davis RJ, Ghosh S, Flavell RA. 2000. Role of the guanosine triphosphatase Rac2 in T helper 1 cell differentiation. *Science* 288:2219–2222.

Li S, Yamauchi A, Marchal CC, Molitoris JK, Quilliam LA, Dinauer MC. 2002. Chemoattractant-stimulated Rac activation in wild-type and Rac2-deficient murine neutrophils: preferential activation of Rac2 and Rac2 gene dosage effect on neutrophil functions. *J Immunol.* 169:5043–5051.

Loisel DA, Rockman MV, Wray GA, Altmann J, Alberts SC. 2006. Ancient polymorphism and functional variation in the primate MHC-DQA1 5' cis-regulatory region. *Proc Natl Acad Sci U S A.* 103:16331–16336.

Lucas M, Zayas MD, De Costa AF, Solano F, Chadli A, Dinca L, Izquierdo G. 2004. A study of promoter and intronic markers of Apol/Fas gene and the interaction with Fas ligand in relapsing multiple sclerosis. *Eur Neurol.* 52:12–17.

Marth GT, Czabarka E, Murvai J, Sherry ST. 2004. The allele frequency spectrum in genome-wide human variation data reveals signals of differential demographic history in three large world populations. *Genetics* 166:351–372.

McDonald WI, Compston A, Edan G, et al. (16 co-authors). 2001. Recommended diagnostic criteria for multiple sclerosis: guidelines from the international panel on the diagnosis of multiple sclerosis. *Ann Neurol.* 50:121–127.

Melum E, Franke A, Schramm C, et al. (43 co-authors). 2011. Genome-wide association analysis in primary sclerosing cholangitis identifies two non-HLA susceptibility loci. *Nat Genet.* 43:17–19.

Nei M, Li WH. 1979. Mathematical model for studying genetic variation in terms of restriction endonucleases. *Proc Natl Acad Sci U S A.* 76:5269–5273.

Nielsen NM, Frisch M, Rostgaard K, Wohlfahrt J, Hjalgrim H, Koch-Henriksen N, Melbye M, Westergaard T. 2008. Autoimmune diseases in patients with multiple sclerosis and their first-degree relatives: a nationwide cohort study in Denmark. *Mult Scler.* 14:823–829.

Plenge R. 2010. GWASs and the age of human as the model organism for autoimmune genetic research. *Genome Biol.* 11:212.

Pritchard JK, Stephens M, Donnelly P. 2000. Inference of population structure using multilocus genotype data. *Genetics* 155:945–959.

Purcell S, Neale B, Todd-Brown K, et al. (11 co-authors). 2007. PLINK: a tool set for whole-genome association and population-based linkage analyses. *Am J Hum Genet.* 81:559–575.

Ramaswamy M, Dumont C, Cruz AC, Muppidi JR, Gomez TS, Billadeau DD, Tybulewicz VL, Siegel RM. 2007. Cutting edge: Rac GTPases sensitize activated T cells to die via Fas. *J Immunol.* 179:6384–6388.

Schaffner SF, Foo C, Gabriel S, Reich D, Daly MJ, Altshuler D. 2005. Calibrating a coalescent simulation of human genome sequence variation. *Genome Res.* 15:1576–1583.

Sironi M, Clerici M. 2010. The hygiene hypothesis: an evolutionary perspective. *Microbes Infect.* 12:421–427.

Sironi M, Menozzi G, Comi GP, Cagliani R, Bresolin N, Pozzoli U. 2005. Analysis of intronic conserved elements indicates that functional complexity might represent a major source of negative selection on non-coding sequences. *Hum Mol Genet.* 14:2533–2546.

Snow AL, Pandiyan P, Zheng L, Krummey SM, Lenardo MJ. 2010. The power and the promise of restimulation-induced cell death in human immune diseases. *Immunol Rev.* 236:68–82.

Stephens M, Scheet P. 2005. Accounting for decay of linkage disequilibrium in haplotype inference and missing-data imputation. *Am J Hum Genet.* 76:449–462.

Stephens M, Smith NJ, Donnelly P. 2001. A new statistical method for haplotype reconstruction from population data. *Am J Hum Genet.* 68:978–989.

Tajima F. 1989. Statistical method for testing the neutral mutation hypothesis by DNA polymorphism. *Genetics* 123:585–595.

Thornton K. 2003. Libsequence: a C++ class library for evolutionary genetic analysis. *Bioinformatics* 19:2325–2327.

Tishkoff SA, Verrelli BC. 2003. Patterns of human genetic diversity: implications for human evolutionary history and disease. *Annu Rev Genomics Hum Genet.* 4:293–340.

van Veen T, Kalkers NF, Crusius JB, van Winsen L, Barkhof F, Jongen PJ, Pena AS, Polman CH, Uitdehaag BM. 2002. The FAS-670 polymorphism influences susceptibility to multiple sclerosis. *J Neuroimmunol.* 128:95–100.

Voight BF, Adams AM, Frisse LA, Qian Y, Hudson RR, Di Rienzo A. 2005. Interrogating multiple aspects of variation in a full resequencing data set to infer human population size changes. *Proc Natl Acad Sci U S A.* 102:18508–18513.

Watterson GA. 1975. On the number of segregating sites in genetical models without recombination. *Theor Popul Biol.* 7:256–276.

Weng X, Liu L, Barcellos LF, Allison JE, Herrinton LJ. 2007. Clustering of inflammatory bowel disease with immune mediated diseases among members of a northern California-managed care organization. *Am J Gastroenterol.* 102:1429–1435.

Wright S. 1950. Genetical structure of populations. *Nature* 166:247–249.

Wright SI, Charlesworth B. 2004. The HKA test revisited: a maximum-likelihood-ratio test of the standard neutral model. *Genetics* 168:1071–1076.

Yu H, Leitenberg D, Li B, Flavell RA. 2001. Deficiency of small GTPase Rac2 affects T cell activation. *J Exp Med.* 194:915–926.

Zayas MD, Lucas M, Solano F, Fernandez-Perez MJ, Izquierdo G. 2001. Association of a CA repeat polymorphism upstream of the Fas ligand gene with multiple sclerosis. *J Neuroimmunol.* 116:238–241.

Zenewicz LA, Abraham C, Flavell RA, Cho JH. 2010. Unraveling the genetics of autoimmunity. *Cell* 140:791–797.

Human Immunology 72 (2011) 295–304

Contents lists available at ScienceDirect

journal homepage: www.elsevier.com/locate/humimm

A recombinant vesicular stomatitis virus encoding HIV-1 receptors and human OX40 ligand efficiently eliminates HIV-1–infected CD4-positive T cells expressing OX40

Chikayuki Tsuruno [a,b], Kazu Okuma [a,*], Yoshiaki Takahashi [c], Reiko Tanaka [d], Yuetsu Tanaka [d], Youichi Takahama [b], Yukio Hamaguchi [b], Isao Hamaguchi [a], Kazunari Yamaguchi [a]

[a] Department of Safety Research on Blood and Biological products, National Institute of Infectious Diseases, Tokyo, Japan
[b] Technology and Product Development Division, Diagnostic Reagent Development, Sysmex Corporation, Kobe, Japan
[c] AIDS Research Center, National Institute of Infectious Diseases, Tokyo, Japan
[d] Department of Immunology, Graduate School and Faculty of Medicine, University of the Ryukyus, Okinawa, Japan

ARTICLE INFO

Article history:
Received 24 August 2010
Accepted 13 December 2010
Available online 21 January 2011

Keywords:
OX40
OX40L
HIV-1–infected cells
VSV targeting

ABSTRACT

OX40 protein is highly expressed on activated CD4-positive T cells that are susceptible for human immunodeficiency virus type 1 (HIV-1) infection. To target and kill HIV-1–infected OX40$^+$ T cells, we used a recombinant vesicular stomatitis virus (rVSV) lacking its envelope glycoprotein (ΔG) and instead expressing HIV-1 receptors CD4/CXCR4 and OX40 ligand (OX40L). Expression of OX40L as well as HIV-1 receptors on the VSV particles led to specific infection of OX40$^+$ T cells, including primary cells, either acutely or chronically infected with X4 HIV-1. Consequently, the rVSV rapidly eliminated these infected cells and caused a marked reduction of HIV-1 viral load in culture. Inclusion of the OX40L gene in the VSV recombinant led to significantly better infection and HIV-1 elimination compared with an rVSVΔG expressing only HIV-1 receptors. A novel rVSVΔG encoding both HIV-1 receptors and OX40L has a potentially greater therapeutic value than an rVSVΔG expressing only HIV-1 receptors.

1. Introduction

The institution of highly active antiretroviral therapy (HAART) has been highly effective in reducing human immunodeficiency virus type 1 (HIV-1) viral loads, significantly prolonging the time interval between infection and the development of acquired immunodeficiency syndrome, and reducing mortality [1,2]. However, there are some clear limitations to HAART-based therapies. Among them is the failure to eradicate persistently/latently HIV-1–infected cell reservoirs. This view has led to a number of studies that have used a variety of complementing or alternative anti-HIV therapeutic strategies. These include the use of immunotoxins [3–5], a recombinant vesicular stomatitis virus (rVSV) [6], pseudotype viruses [7,8] and armed NK cells [9], each aimed at targeting the elimination of HIV-1–infected cells.

Human OX40 (CD134) is a type I transmembrane protein expressed primarily on activated T cells and is a member of the tumor necrosis factor receptor superfamily [10–12]. Human OX40 ligand (OX40L, CD252) is a type II transmembrane protein expressed by several cell types, including activated dendritic cells and belongs to the TNF superfamily [13–17]. In context of the present studies, OX40-OX40L interaction promotes cell–cell adhesion between activated CD4$^+$ T cells and vascular endothelial cells [18] and migration of CD4$^+$ T cells to B cell follicles in peripheral lymph nodes [19]. In addition, several members of the TNF superfamily have been shown to promote cell death [20]. It is notable that the ligation of OX40 by OX40L induces apoptotic cell death in co-cultures of a number of cell lines expressing this pair of cognate receptor/ligand [21,22].

Thus, we reasoned that OX40 could serve as a novel therapeutic target for anti-HIV therapy since it is expressed at relatively high mean densities on activated CD4$^+$ T cells that are selectively more permissive to HIV-1 infection/propagation. Given that OX40 functions as an adhesion molecule with OX40L, it seemed logical to capitalize the rVSV targeting X4 HIV-1–infected cells and generate an rVSV additionally expressing OX40L on the viral surface to enhance the efficiency of infection of HIV-1–infected OX40$^+$ cells. Such an rVSV was thus generated in this study and examined for its antiviral potential *in vitro*.

2. Subjects and methods

2.1. Cells and virus

BHK-21 cells (Riken BRC Cell Bank, Tsukuba, Japan) were grown in Dulbecco's modified Eagle's medium (Sigma-Aldrich, St. Louis, MO) supplemented with 10% fetal bovine serum and and 1% Antibiotic-

* Corresponding author.
E-mail address: kokuma@nih.go.jp (K. Okuma).
Y. Takahashi is currently at the Department of Pathology and Laboratory Medicine, Emory University School of Medicine, Atlanta, Georgia.
C. Tsuruno and K. Okuma, contributed equally to this work.

0198-8859/11/$32.00 - see front matter © 2011 American Society for Histocompatibility and Immunogenetics. Published by Elsevier Inc. All rights reserved.
doi:10.1016/j.humimm.2011.01.007

Antimycotic (Gibco, Carlsbad, CA) solution. BHK-G cells [6] (provided by Dr Rose) were cultured in DMEM supplemented with 10% FBS, 750 μg/ml geneticin, and 0.5 μg/ml tetracycline [23]. Expression of VSV G by BHK-G cells was induced by transferring cells to a tetracycline-free DMEM. The parent 293T cells and 293T cells transfected with and stably expressing OX40 (293T/OX40) were grown in Iscove's modified Dulbecco's medium (Sigma-Aldrich) supplemented with 10% FBS and 1% Antibiotic-Antimycotic solution. The Molt-4 cell line transfected with and stably expressing OX40 (Molt-4/OX40) [22] and the Molt-4/OX40 cell line persistently infected with HIV-1_{IIIB} (Molt-4/IIIB/OX40) [22] were cultured in RPMI-1640 medium (Sigma-Aldrich) supplemented with 10% FBS and 1% Antibiotic-Antimycotic solution.

Primary $CD4^+$ T cells were isolated from peripheral blood mononuclear cells obtained from a healthy donor by a MACS negative selection kit (Miltenyi Biotec, Gladbach, Germany) and activated every 3 days using anti-CD3/CD28-conjugated Dynabeads (Invitrogen, Carlsbad, CA) in RPMI-1640 medium supplemented with 10% FBS, 1% Antibiotic-Antimycotic solution, 20 U/ml recombinant human interleukin (rhIL)-2 (Shionogi Pharmaceutical, Osaka, Japan) and 20 ng/ml rhIL-4 (Peprotec, London, UK). Primary $CD4^+$ T cells initially stimulated for 3 days with anti-CD3/CD28 immunobeads were washed and then infected with recombinant X4 HIV-1–expressing enhanced green fluorescent protein (EGFP) as described below. Two days later an aliquot of these primary cells was incubated in a 1:10 dilution of a phycoerythrin-conjugated mouse anti-OX40 monoclonal antibody (clone B-7B5) [16,21] at 4°C for 30 minutes, washed, and analyzed to determine the frequency of HIV-1–infected ($EGFP^+$) and $OX40^+$ cells by flow cytometry using a FACSCalibur (Becton Dickinson, Franklin Lakes, NJ).

A recombinant virus derived from HIV-1_{NL4-3}, NL-EGFP strain [24], that was engineered to express EGFP upon infection was produced by transient transfection of 293T cells with an expression plasmid containing this construct (provided by Dr Koyanagi). HIV-1 p24 levels of the viral stocks were determined with an enzyme-linked immunosorbent assay kit (Zepto Metrix, Buffalo, NY).

2.2. Plasmid construction

To construct an rVSV plasmid lacking the G gene and encoding human OX40L in addition to human CD4/CXCR4, the OX40L gene was first amplified by PCR from the expression vector pSGP34-1 [14] with Vent polymerase (New England Biolabs, Ipswich, MA) using a forward primer 5′-GATCGGGCCC**CCTAGG**TATGAAAAAAACTAACAGTAATCAAAATGGAAAGGGTCCAACCCCTGGAAG-3′ and a reverse primer 5′-AAGGAAAAAA**GCGGCCGC**TCAAAGGACACAGAATTCACCAGGATTTTGATGGATAAGAATCAGTTC-3′. The forward primer contained an *Avr*II site (bold) and a VSV transcription stop-start signal (underlined). The reverse primer contained a *Not*I site (bold). Next, the PCR product was digested with *Avr*II and *Not*I and cloned into pVSVΔG-CC4 [6] encoding CD4/CXCR4 instead of G (a gift from Dr Rose) that had been digested with the same enzymes, yielding pVSVΔG-CC4XL.

2.3. Isolation of VSV recombinants

An rVSVΔG expressing CD4, CXCR4 and OX40L (termed VSVΔG-CC4XL) was isolated according to established methods [25,26]. Briefly, 1 million BHK-21 cells were dispensed into each 10-cm-diameter dish, and the cells were then infected with vTF7-3 [27] at a multiplicity of infection of 10. One hour later these cells were transfected with 10 μg of pVSVΔG-CC4XL described above and helper plasmids using the *Trans*IT-LT1 reagent (*Mirus*, Madison, WI) and incubated at 37°C for 48 hours. Culture supernatants were then harvested from the dishes, passed through filters to remove vTF7-3 and transferred to fresh BHK-G cells expressing the induced G. Culture supernatants harvested were diluted in FBS-free DMEM, and then added to BHK-G cells expressing the induced G in Minimum Essential Medium (Invitrogen) containing 10% FBS, 1% Antibiotic-Antimycotic and 1% methylcellulose. Following infection, individual plaques isolated from the cells were grown on fresh BHK-G cells expressing the induced G again. Such plaque-purified viruses were then titrated on BHK-G cells expressing the induced G in MEM containing methylcellulose, and titers were determined as PFU/ml. VSVΔG and VSVΔG-CC4 were prepared as previously reported [6,28].

G-complemented rVSVs mentioned above were incubated with a total of 1×10^6 BHK-21 cells seeded onto a 6-well plate at an MOI of 1. After adsorption of the viruses, the supernatant fluid was aspirated and the cells were washed with FBS-free DMEM at least twice to remove residual input viruses. The cells were then incubated in fresh complete DMEM at 37°C for 24 hours and the culture media were used as non–G-complemented viruses.

2.4. Indirect immunofluorescence

A total of 50,000 293T cells seeded into each well of an eight-well Lab-Tek II chamber slide (Nunc, Rochester, NY) were transfected with or without the expression plasmids for X4 HIV-1 Env (HXB2-env) [29] and Rev [30] using Lipofectamine LTX with PLUS reagent (Invitrogen). Two days later the 293T cells were incubated with an equal volume of media containing VSVΔG, VSVΔG-CC4, or VSVΔG-CC4XL. Control consisted of cells that were mock-infected. After 15 hours' infection, the cells were fixed in phosphate-buffered saline containing 4% paraformaldehyde, washed in PBS containing 20 mmol/l glycine (PBS-Glycine) and permeabilized with 1% Triton X-100 in PBS-Glycine. The cells were then incubated in a 1:5 dilution of a mouse anti-VSV nucleoprotein (N) mAb (clone 10G4; courtesy of Dr Lyles) [31] at 37°C for 20 minutes, washed, and then incubated with a 1:50 dilution of a fluorescein isothiocyanate–conjugated goat anti-mouse Ab (Beckman Coulter, Brea, CA) at 37°C for 20 minutes. After washing in PBS-Glycine, the cells were observed by fluorescence microscopy and the expression of VSV N protein in the cells was visualized as a measure of VSV infection. To compare infectivity of each rVSV, the total number of fluorescent (VSV-infected) cells in each well were counted and the percentage infectivity calculated.

2.5. Cell fusion assay

Molt-4/IIIB/OX40 cells (1×10^5) were seeded in each well of a 96-well plate and mock-infected or superinfected with 15 μl of VSVΔG, VSVΔG-CC4, or VSVΔG-CC4XL to test whether the expression of OX40L induced by VSVΔG-CC4XL infection affected cell fusion. In parallel, to examine if the neutralizing anti-OX40L mAb (5A8) [21,22] efficiently blocked the effect of OX40L on cell fusion activity through binding to OX40, either VSVΔG-CC4 or VSVΔG-CC4XL was preincubated with 10, 20, 50, or 100 μg/ml of anti-OX40L or an isotype-identical control mouse mAb at 37°C for 1 hour followed by infection with the rVSV constructs. After incubation for 15 hours, the cells were observed under the microscope. To quantify cell fusion induced by rVSV infection, the numbers of syncytia within 3 random fields were determined. In addition, the percentage cell fusion inhibited by the addition of anti-OX40L mAb at each concentration was calculated.

2.6. Detection of HIV-1–infected cells after VSV infection

To evaluate the killing effect of rVSVs on X4 HIV-1 persistently infected cells, 1×10^6 Molt-4/IIIB/OX40 cells were washed, seeded in each well of a 12-well plate, and then mock-infected or superinfected with 500 μl of VSVΔG, VSVΔG-CC4 or VSVΔG-CC4XL. As a control experiment, to determine the killing effect of rVSVs on HIV-1-uninfected $OX40^+$ cells, 2.5×10^5 Molt-4/OX40 cells in each well of a 12-well plate were mock-infected or infected with 500 μl

of VSVΔG-CC4 or VSVΔG-CC4XL. While the cells were incubated for 8 days, a portion (10%) of the culture medium was collected from each well daily and replaced by an equal volume of fresh medium. The standard Trypan-blue dye exclusion technique was utilized for determining the frequency of live (HIV-1–infected) cells using a hemocytometer. The data are reported as % cell viability at each time point relative to the total cell number at the starting time point.

To evaluate the killing effect of rVSVs on cells acutely infected with X4 HIV-1, 2.5×10^5 Molt-4/OX40 cells or 7.0×10^4 primary day 3 anti-CD3/CD28-activated $CD4^+$ T cells were seeded in each well of a 12-well plate, and a stock of NL-EGFP strain containing 80 ng p24 was inoculated into each well. At 2 days after HIV-1 infection, the cells were mock-infected or superinfected with 500 μl of either VSVΔG-CC4 or VSVΔG-CC4XL (or with either G-complemented rVSV at an MOI of 0.1). The infection was followed for an additional 3 days. As a control for the determination of EGFP-negative cells, neither NL-EGFP nor rVSV was inoculated to the control culture. The culture medium was collected from each well at each time point, and the cultures replenished with the same amount of fresh media. The cells obtained were then fixed and viable cells were analyzed by flow cytometry to detect $EGFP^+$ (NL-EGFP–infected) cells. The data obtained are reported as percentage of control values derived on viable mock-infected cells collected at each time point.

2.7. Determination of HIV-1 viral load in culture

For the determination of HIV-1 viral loads, aliquots of the culture medium collected at each time point were analyzed for p24 levels using a commercially available ELISA kit.

Furthermore, when either Molt-4/IIIB/OX40 cells or NL-EGFP acutely infected Molt-4/OX40 cells were mock-infected or superinfected with rVSVs, HIV-1 titers in the culture supernatants were determined as follows. After VSV infection, aliquots of the culture supernatants obtained every other day were serially diluted and dispensed into Molt-4/OX40 cells (1×10^4 per well) seeded in 96-well plates. The plates were incubated at 37°C for 5–7 days and p24 levels in the supernatant fluid quantitated using the ELISA kit and the frequency of $EGFP^+$ cells determined by fluorescence microscopy. The titers for each of the assays were determined by end-point titration and are reported as infectious units per milliliter.

2.8. Statistical analysis

The data presented herein were analyzed using the Student *t* test with GraphPad Prism (version 4.0c for Windows XP; GraphPad Software).

3. Results

3.1. Construction and isolation of VSVΔG-CC4XL

With the aim of developing a novel anti-HIV-1 therapeutic agent, a strategy for targeting HIV-1–infected $CD4^+$ T cells through OX40-OX40L interaction was considered. In the studies reported here, the rVSV the G gene of which was replaced with the X4 HIV-1 receptors, CD4 and CXCR4, termed VSVΔG-CC4 (Fig. 1), was used, as cells transfected with and expressing this recombinant were previously reported to be cytotoxic for X4 HIV-1–infected target cells via Env-receptor interactions [6]. It was reasoned that the inclusion of OX40L protein in addition to CD4 and CXCR4 and expressed on the membrane of cells transfected with VSVΔG-CC4XL (Fig. 1) may increase the efficiency of VSV targeting and superinfecting HIV-1–infected cells through binding of OX40L to its cognate receptor OX40 expressed on the cell surface of HIV-1–infected target cells. Figure 1 summarizes the various constructs prepared as described in the Subjects and methods section and used in the studies reported here, including the control constructs.

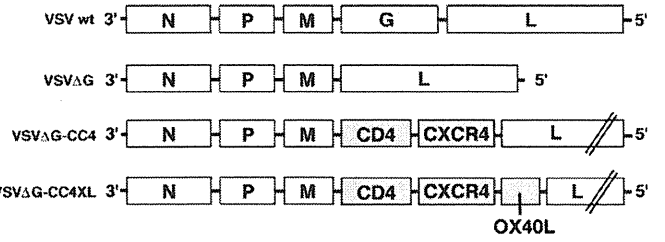

Fig. 1. Schematic structure of the rVSVs used. The order of the genomes of the rVSV constructs used in the studies, including the wild-type construct, is displayed. The VSVΔG construct is G gene-deleted, which was replaced with the genes encoding human CD4 and CXCR4 inserted between the M and L genes of the VSVΔG genome. In addition, the gene encoding human OX40L was cloned downstream of the CXCR4 gene in the VSVΔG-CC4 genome, yielding the VSVΔG-CC4XL construct. Expression of the OX40L protein after infection was confirmed by indirect immunofluorescence.

3.2. Efficient infection of Env-expressing $OX40^+$ cells with VSVΔG-CC4XL

In an effort to determine the effects of OX40L co-expression in addition to CD4 and CXCR4 by the VSVΔG-CC4XL-transfected cells, we first examined its infectivity using HIV-1 Env-expressing $OX40^+$ target cells. 293T/OX40 cells were transfected with the expression plasmids for X4 HIV-1 Env and Rev, and then aliquots were either mock-infected or infected with an equal volume of VSVΔG, VSVΔG-CC4, or VSVΔG-CC4XL. Additional controls included the use of the nontransfected 293T/OX40 cells infected with the various constructs. After 15 hours infection, the cells were tested by immunofluorescence using anti-VSV N mAb, followed by FITC-conjugated anti-mouse IgG. As shown in Fig. 2A, whereas the mock-infected cells did not express the N protein and VSVΔG did not infect Env-expressing 293T/OX40 cells, the VSVΔG-CC4 and VSVΔG-CC4XL constructs both showed clear evidence of infection in these cells. Importantly, microscopic quantification showed that the VSVΔG-CC4XL construct led to an eightfold higher frequency of infected cells compared with the VSVΔG-CC4 construct (Fig. 2B). In contrast, non–Env-expressing 293T/OX40 cells were not susceptible to infection with the rVSVs tested (Fig. 2A). These results confirm that infection of cells with rVSVs expressing HIV-1 receptors instead of G is Env-dependent and suggest that the enhancement of infectivity was most likely mediated by the interaction between OX40 at the cell surface and OX40L incorporated into the envelope of VSV particles.

3.3. Enhanced cell fusion induced by infection of HIV-1–infected $OX40^+$ cells with VSVΔG-CC4XL

We reasoned that the inclusion of the OX40L molecule with CD4 and CXCR4 expressed on the cells infected by the rVSV might enhance the cell fusion process following interaction with Env-expressing $OX40^+$ cells. To test this possibility, we mock-infected or infected aliquots of the Molt-4/IIIB/OX40 cell line with equal volumes of either VSVΔG, VSVΔG-CC4 or VSVΔG-CC4XL and 15 hours later the cells were observed by microscopy. In addition, for purposes of controls, we included infection of aliquots of the Molt-4/OX40 cell line with the same rVSV constructs. As seen in Fig. 3A, infection of Molt-4/IIIB/OX40 cells with either VSVΔG-CC4 or VSVΔG-CC4XL induced significant syncytia, whereas infection of cells with either mock or VSVΔG did not lead to detectable levels of syncytia-forming cells (Fig. 3A, upper and middle panels). Once again, not only did infection of the cells with the VSVΔG-CC4XL construct increase the number of syncytia, but the syncytia were also significantly larger than those induced using the VSVΔG-CC4 construct (Fig. 3A, middle panels). In contrast, no

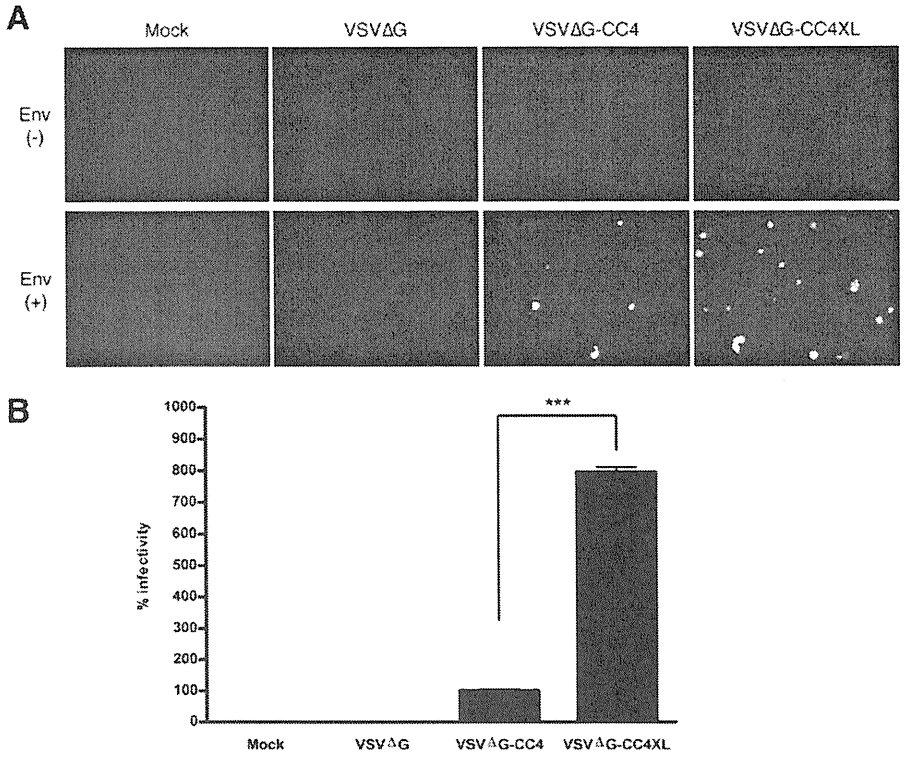

Fig. 2. In vitro infectivity of the rVSVs in cells expressing both the X4 HIV-1 Env and the OX40 protein. (A) The 293T/OX40 cells were initially transfected with or without an expression plasmid for X4 HIV-1 Env for 2 days. The Env-expressing [Env (+)] or non–Env-expressing [Env (−)] $OX40^+$ cells were either mock-infected or infected with VSVΔG, VSVΔG-CC4, or VSVΔG-CC4XL. After 15 hours' incubation, the cells were fixed and examined by indirect immunofluorescence (×100 magnification) using a mouse anti-VSV N mAb followed by a FITC-conjugated anti-mouse IgG to detect VSV-infected cells. The stained cells were observed by fluorescence microscopy with an Olympus IX-FLA apparatus, and photographs of the cells were taken with an Olympus DP71 digital camera using an Olympus IX70 microscope. (B) The relative infectivity of each virus was quantified by enumerating the total number of fluorescent cells per well and by determining the frequency of VSV-infected cells relative to VSVΔG-CC4–infected cultures. The cultures were performed in triplicates and the data expressed as % infectivity (mean + SE). The data obtained were also analyzed by Student's *t* test and the percent infectivity of the VSVΔG-CC4XL construct was determined to be significantly higher than that of the VSVΔG-CC4 construct (denoted by ***, $p < 0.001$). Representative data from one of three independent experiments are shown.

detectable syncytia were noted when the Molt-4/OX40 cells were mock-infected or infected with either of the rVSV constructs (data not shown).

Furthermore, in efforts to determine if the enhancement in cell fusion was mediated by specific interaction between OX40 and its cognate ligand, use was made of an anti-OX40L neutralizing mAb (5A8). Aliquots of the Molt-4/IIIB/OX40 cells were thus incubated with either the VSVΔG-CC4 or the VSVΔG-CC4XL construct that was pretreated with the indicated concentrations of the anti-OX40L mAb. Treatment of aliquots of the same rVSV constructs with an isotype control mAb was used as a control. After 15 hours, the numbers of syncytia induced by each rVSV construct were enumerated under the microscope. As seen in Fig. 3A (lower panels), there was a marked reduction in the frequency of syncytia in Molt-4/IIIB/OX40 cells incubated with VSVΔG-CC4XL preincubated with the anti-OX40L mAb, compared with preincubation of the cells with the isotype control mAb. Additionally, augmentation in the frequency of cell fusions by VSVΔG-CC4XL infection was inhibited by pretreatment with the anti-OX40L mAb in a dose-dependent manner (Fig. 3B). As expected, pretreatment of VSVΔG-CC4 with either the anti-OX40L or the control mAb did not affect the induced cell fusion (Fig. 3B). These data suggest that the major contributor for the augmentation of cell fusion was due to the interaction between the OX40 molecule and its cognate ligand. These findings also indicate that the OX40L protein expressed by VSVΔG-CC4XL was functional because of the marked increase in the efficiency of not only the rVSV infection but also the rVSV-induced cell fusion.

3.4. Elimination of cells chronically infected with HIV-1 by VSVΔG-CC4XL infection is associated with a reduction of HIV-1 viral load

The above findings of the high efficiency of infection noted using the VSVΔG-CC4XL construct early postinfection prompted us to carry out studies to determine the potential of this construct to induce cytotoxicity and to inhibit HIV-1 production upon prolonged culture of the superinfected cells.

An initial experiment was carried out in efforts to determine whether VSVΔG-CC4XL elicited a cytotoxic effect on HIV-1 Env-negative $OX40^+$ T cells. Aliquots of Molt-4/OX40 cells were infected with either VSVΔG-CC4 or VSVΔG-CC4XL and for purposes of control mock-infected, and then the number of live cells were counted daily for a total of 8 days. As shown in Fig. 4A, VSVΔG-CC4XL had a marginal effect compared with mock and VSVΔG-CC4 all through the time of culture.

Thus, after aliquots of HIV-1 Env^+ $OX40^+$ Molt-4/IIIB/OX40 cells were washed, equal volumes of VSVΔG, VSVΔG-CC4, or VSVΔG-CC4XL were added to the cells. A control culture was left uninfected with rVSV (mock-infected). A portion of replicate cultures representing each combination was harvested daily for a total of 8 days and the number of viable cells determined. As shown in Fig. 4B, after superinfection with either VSVΔG-CC4 or VSVΔG-CC4XL, the percentage of live cells began to decrease immediately and rapidly (approximately 40% and 10% on day 1) with 2–5% thereafter and <1% by day 3, respectively. In cells mock-infected or infected with VSVΔG, the percentage of live cells continued to increase and reached around 400% by day 4 and day 6, respectively, and then began to decrease gradually. These data not only document the

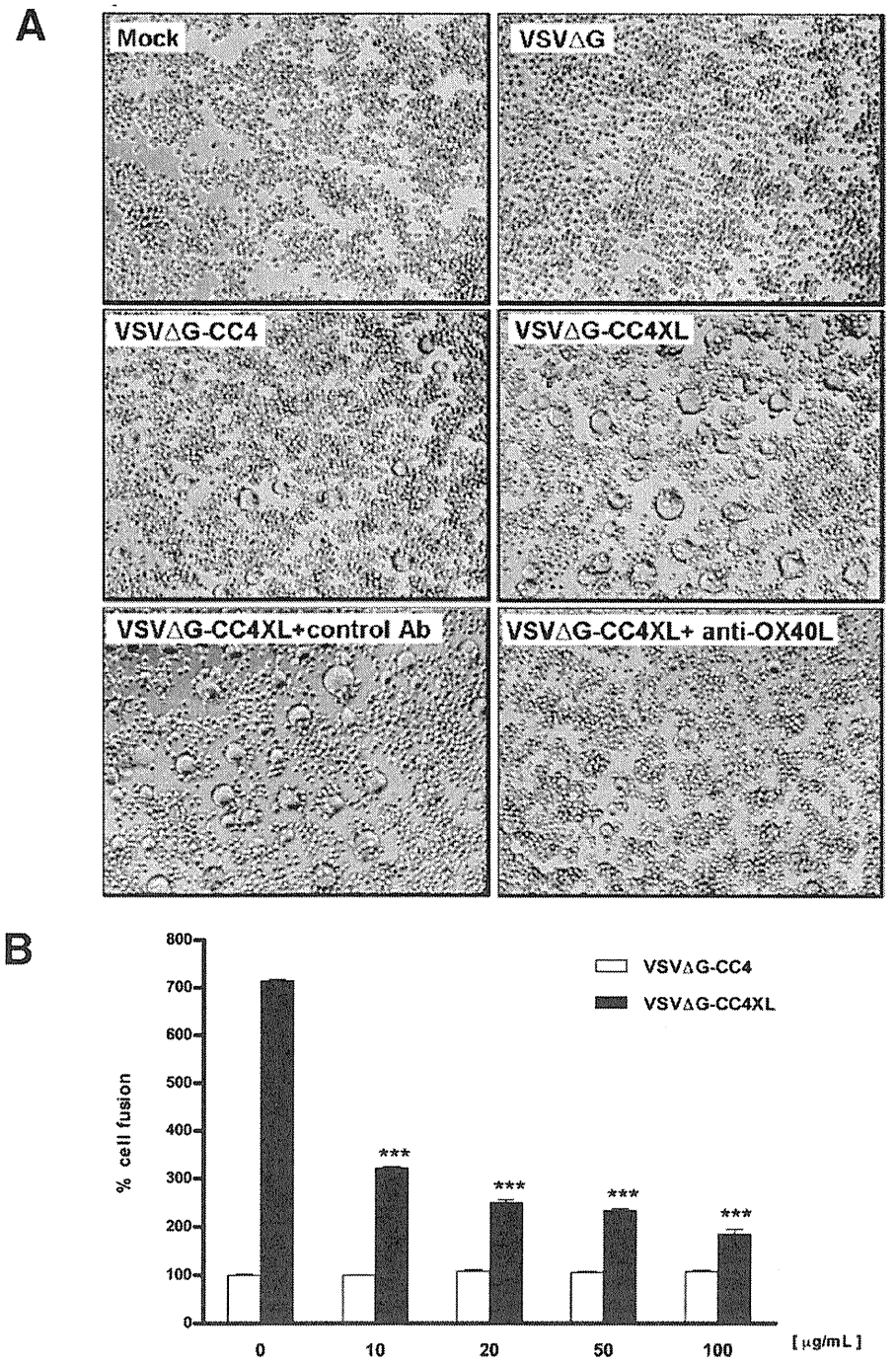

Fig. 3. Induction of cell fusion by superinfection of HIV-1–infected cells with the rVSVs. (A) The Molt-4/IIIB/OX40 cells were mock-infected or superinfected with VSVΔG, VSVΔG-CC4, or VSVΔG-CC4XL. After incubation for 15 hours, the cells were observed under the Olympus CKX41 microscope and photographed by a Nikon DS-5M digital camera at ×100 magnification. Representative images of the mock-infected cells (top left), the VSVΔG superinfected cells (top right), and the cultures superinfected with VSVΔG-CC4 or VSVΔG-CC4XL (middle) are shown. In addition, aliquots of the cultures superinfected with the VSVΔG-CC4XL construct pretreated with 20 μg/ml of the anti-OX40L mAb (bottom right) or the control mAb (bottom left) are displayed. (B) Either VSVΔG-CC4 or VSVΔG-CC4XL was pretreated with the anti-OX40L mAb at the concentrations indicated and subsequently incubated with aliquots of the Molt-4/IIIB/OX40 cells. Fifteen hours later, the superinfected cells were observed by microscopy and the numbers of syncytia were counted. This assay was performed in triplicate. The data shown are reported as percent cell fusion noted in cultures superinfected with the VSVΔG-CC4 construct pretreated without the mAb (mean + SE). The data obtained were also analyzed by Student's *t* test. The values obtained in cultures incubated with VSVΔG-CC4XL pretreated with the anti-OX40L mAb at each concentration were significantly different from the values noted in cultures incubated with VSVΔG-CC4XL pretreated without the mAb (denoted by ***, $p < 0.001$). Representative results from one of three independent experiments are shown.

effectiveness of VSVΔG-CC4XL and VSVΔG-CC4 for lysing the target cells but also demonstrate the higher relative efficiency of the former than that of the latter on mediating the lytic effect.

Supernatant fluids from such cultures were also analyzed for levels of p24. As seen in Fig. 4C, supernatant fluids from the mock-infected cultures or those infected with VSVΔG showed robust p24 levels that reached plateau levels at approximately 1500 ng/ml. In contrast, p24 levels in the cultures superinfected with VSVΔG-CC4 or VSVΔG-CC4XL peaked at approximately 150 ng/ml on day 2 after infection and then declined down to approximately 50–90 ng/ml by day 8. Throughout this assay, infection with the VSVΔG-CC4XL construct inhibited p24 production more efficiently than that with

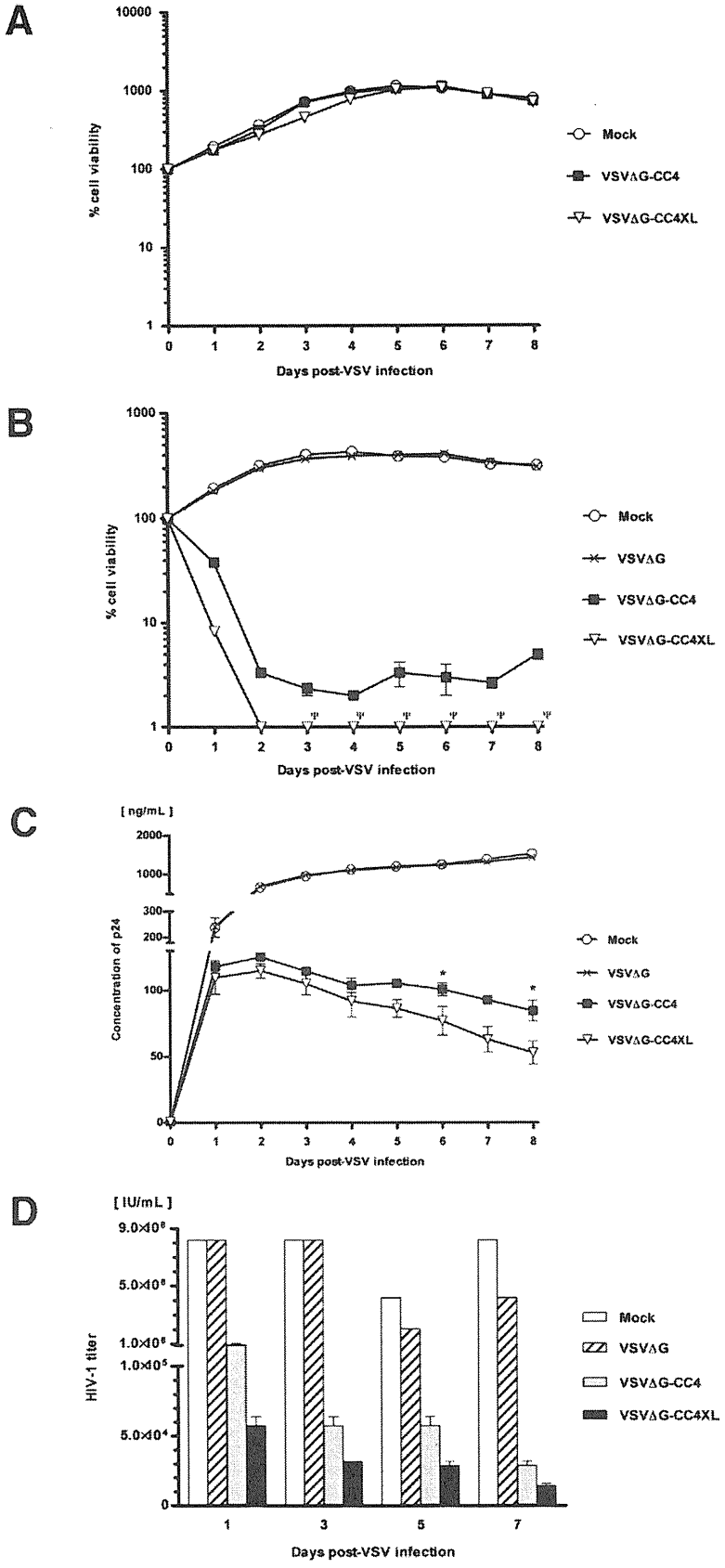

Fig. 4. Depletion of HIV-1 chronically infected target cells by superinfection with the rVSVs results in reduction of HIV-1 viral load. Aliquots of the Molt-4/IIIB/OX40 cells were washed and then mock-infected or superinfected with VSVΔG, VSVΔG-CC4 or VSVΔG-CC4XL. As a control, aliquots of the Molt-4/OX40 cells were mock-infected or superinfected with either VSVΔG-CC4 or VSVΔG-CC4XL. A fraction of triplicate culture from each combination was harvested daily for a total of 8 days, and the number of viable cells determined using Trypan blue dye exclusion and the supernatant fluids of Molt-4/IIIB/OX40 cell culture assayed for the level of HIV-1 p24 by ELISA. (A) Percent viability of the Molt-4/OX40 cells (mean ± SE). (B) Percent viability of the Molt-4/IIIB/OX40 cells (mean ± SE). The indicated symbol Ψ represents below the level of detection. (C) Levels of p24 (mean ± SE) as determined in the supernatant fluids. The data obtained were also analyzed by Student's *t* test, and the values in the supernatant fluid of

the VSVΔG-CC4 construct with marked differences ($p < 0.05$) noted at days 6 and 8 postinfection (Fig. 4C).

In efforts to confirm the effects of the marked reduction of p24 synthesis, supernatant fluids from the same cultures were assayed for levels of viral titers as outlined in the Subjects and methods section. As seen in Fig. 4D, supernatant fluids from the mock-infected or VSVΔG-infected cultures showed titers that fluctuated between 1.0×10^6 and 8.0×10^6 IU/ml after infection. However, the titers in the supernatant fluids collected from cultures superinfected with VSVΔG-CC4 or VSVΔG-CC4XL decreased to around 1.0×10^6 and 6.0×10^4 IU/ml on day 1 post-infection (eightfold and >100-fold inhibition in comparison with mock infection), respectively. Subsequently the titers continued to decline and reached about 3.0×10^4 and 1.5×10^4 IU/ml on day 7 (>200-fold and >500-fold inhibition relative to mock infection), respectively. These data therefore confirmed the results obtained with the monitoring of p24 levels and underscore the antiviral effect of the VSVΔG-CC4XL construct.

3.5. Assessment of the therapeutic potential of VSVΔG-CC4XL in a T-cell line acutely infected with HIV-1

In efforts to determine whether use could be made of the VSVΔG-CC4XL construct as a therapeutic agent, cell cultures acutely infected with X4 HIV-1 NL-EGFP strain were used. In this assay, the Molt-4/OX40 instead of the Molt-4/IIIB/OX40 cell line was used to minimize a role for the HIV-1 Env. The Molt-4/OX40 cell line was initially infected with the NL-EGFP for 2 days and then aliquots incubated with equal volumes of either VSVΔG-CC4 or VSVΔG-CC4XL. Controls consisted of NL-EGFP–infected cultures that were not superinfected with rVSV (mock-infected) and of cells cultured with neither the NL-EGFP nor the rVSV. A fraction from replicate cultures was harvested daily for 3 days. The cells were subjected to flow cytometric analysis for the frequency of $EGFP^+$ (HIV-1–infected) cells and the supernatant fluids used to determine the levels of HIV-1. It should be noted that HIV-1 infection of the cultures in general leads to a reduction in the number of cells because of the lytic action of the replicating virus. Thus, data presented are a reflection of the net effects and depicted as % of control values of $EGFP^+$ cells in the mock-infected cultures. As shown in Fig. 5A, superinfection with VSVΔG-CC4 or VSVΔG-CC4XL led a net decrease in the frequency of $EGFP^+$ cells with values of 70% and 40% of control values, respectively, on day 3 post-VSV infection. Once again, the data clearly demonstrate the higher efficiency of VSVΔG-CC4XL compared with VSVΔG-CC4 in eliminating HIV-1–infected cells.

The supernatant fluids collected from the same cultures were assayed for p24 levels. As seen in Fig. 5B, supernatant fluids from the cultures mock-infected or superinfected with VSVΔG-CC4 showed increasing p24 levels which reached around 500 or 300 ng/ml, respectively, on day 2 post-VSV infection. In contrast, throughout this assay p24 levels in the cultures superinfected with VSVΔG-CC4XL were lower (~100 ng/ml) than those in the other cultures with significant differences ($p < 0.01$ and $p < 0.05$, respectively) noted on day 2.

Furthermore, the supernatant fluids collected from the same cultures were assayed for HIV-1 viral titers. As seen in Fig. 5C, whereas the titers in supernatant fluids from the cells mock-infected or superinfected with VSVΔG-CC4 increased from around 0.5×10^5 IU/ml on day 0 to about 3.0×10^5 IU/ml on day 1 post-VSV infection, the supernatant fluids from the cultures superinfected with VSVΔG-CC4XL showed titers of approximately 0.3×10^5 IU/ml on day 1 (10-fold reduction). In addition, whereas the supernatant fluids from the mock-infected cells continued to show high titers on day 3, those from the VSVΔG-CC4-infected or VSVΔG-CC4XL-infected cultures showed remarkably reduced titers of 0.3×10^5 or 0.1×10^5 IU/ml on the same day (10-fold or 30-fold lower than mock infection), respectively. These findings once again indicate that VSVΔG-CC4XL is more effective at reducing HIV-1 viral load than VSVΔG-CC4, most likely due to increased ability both to detect and kill cells infected with HIV-1 acutely as well as chronically.

3.6. Therapeutic potential of VSVΔG-CC4XL in primary $CD4^+$ T cells acutely infected with HIV-1

Finally, efforts were made to determine the potential of VSVΔG-CC4XL as a therapeutic agent in primary $CD4^+$ T cells acutely infected with HIV-1 instead of the use of transformed T-cell lines. Primary $CD4^+$ T cells were initially activated for 3 days and then infected with NL-EGFP strain. At 2 days postinfection the frequency of $EGFP^+$ (HIV-1–infected) and $OX40^+$ cells was analyzed by flow cytometry. This analysis revealed that more than 1% of the entire live cell population were $EGFP^+$ and approximately two thirds of the $EGFP^+$ cells were $OX40^+$. These findings prompted us to inoculate rVSVs at the same time the cells were infected with HIV-1. These cells were thus superinfected with G-complemented VSVΔG-CC4 or VSVΔG-CC4XL at an MOI of 0.1. As controls, NL-EGFP–infected cultures that were not superinfected with rVSV (mock-infected) and cells cultured with neither the NL-EGFP nor the rVSV were prepared. Culture medium from replicate cultures was harvested daily for 3 days. The cells were analyzed by flow cytometry again for the frequency of $EGFP^+$ cells and the supernatant fluids used to determine the levels of HIV-1 p24.

As seen in Fig. 6A, superinfection with VSVΔG-CC4 or VSVΔG-CC4XL led a decrease in the frequency of $EGFP^+$ cells with values of 81% or 69% of control values on day 2 post-VSV infection, and 71% or 63% on day 3, respectively. Further, Fig. 6B showed that supernatant fluids from the cultures mock-infected or superinfected with VSVΔG-CC4 or VSVΔG-CC4XL exhibited increasing p24 levels which reached 177, 85, or 72 ng/ml, respectively, on day 3 post-VSV infection. These data repeatedly demonstrate the higher efficiency of VSVΔG-CC4XL compared with VSVΔG-CC4 both in eliminating HIV-1–infected cells and in reducing HIV-1 viral load. These results clearly indicate that VSVΔG-CC4XL has a greater therapeutic potential than VSVΔG-CC4 against HIV-1 infection not only of transformed cell lines but also of primary cells.

4. Discussion

Results of our present study demonstrate that OX40 engagement with rVSVΔG expressing HIV-1 receptors in addition to OX40L (VSVΔG-CC4XL) enhanced the killing effect of rVSVΔG expressing HIV-1 receptors alone (VSVΔG-CC4) on HIV-1–infected cells. This finding indicates that OX40-OX40L interactions not only promote cellular adhesion but also apoptotic cell death, as previously reported [18,21,22]. In addition, the expression of OX40L additionally enhanced both rVSV infectivity and cell death compared with values obtained by rVSV infection alone, respectively.

The failure of the VSVΔG-CC4 construct to completely reduce the number of X4 HIV-1 persistently infected Molt-4/IIIB/OX40 cells in contrast to the success of the VSVΔG-CC4XL construct to more efficiently eliminate the cells (Fig. 4B) needs to be addressed. We hypothesize that there could be a low frequency (~5%) of cells

cultures incubated with VSVΔG-CC4 compared with VSVΔG-CC4XL were significantly different (denoted by *, $p < 0.05$). (D) Aliquots of the supernatant fluids obtained at the indicated time points were serially diluted twofold and subsequently inoculated into the Molt-4/OX40 cells. At 7 days post-culture, levels of p24 in the supernatant fluids were quantitated by ELISA. The titers of HIV-1 were determined by end-point titration and are reported as IU/ml calculated. The data shown are mean + SE of the values of the triplicates. The results displayed are representative of one of three independent experiments.

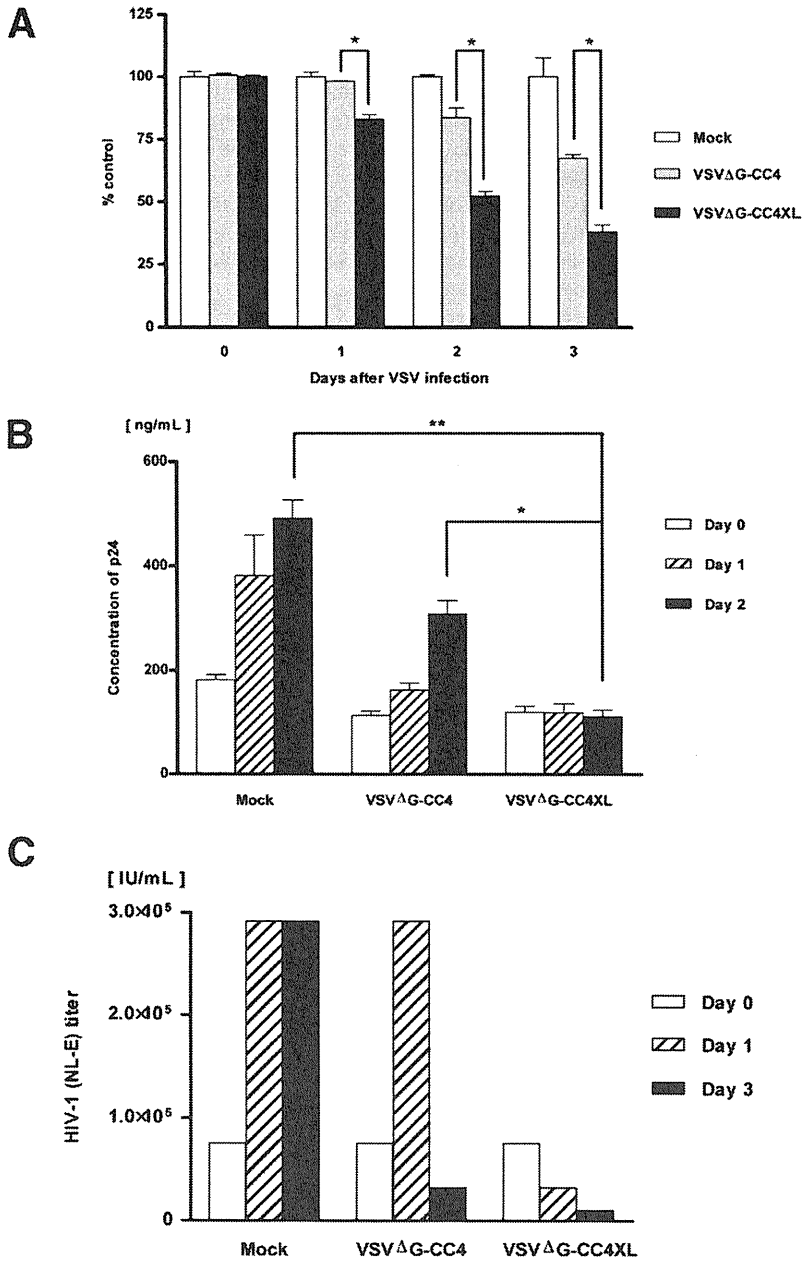

Fig. 5. Effects of the rVSVs on an OX40-expressing CD4$^+$ T cell line acutely infected with HIV-1. The Molt-4/OX40 cells were initially infected for 2 days with the recombinant X4 HIV-1 encoding EGFP. Aliquots of such infected cells were mock-infected or superinfected with either VSVΔG-CC4 or VSVΔG-CC4XL. The co-infected triplicate cultures were incubated for an additional 3 days. A portion (10%) of each culture was harvested daily and the cells and supernatant fluid assayed. The data obtained were analyzed by Student's *t* test. (A) The frequency of EGFP-positive (HIV-1–infected) cells was analyzed by flow cytometry daily after VSV infection. The results shown represent percentage of control values (mean + SE). The values obtained in cultures superinfected with VSVΔG-CC4 were significantly different from the values obtained in cultures superinfected with VSVΔG-CC4XL (denoted by *, $p < 0.05$). (B) Aliquots of the supernatant fluids obtained until day 2 post-VSV infection were assayed by ELISA to determine levels of HIV-1 p24. The results shown represent percentage of control values (mean + SE). The values obtained in cultures superinfected with VSVΔG-CC4 were significantly different from the values obtained in cultures superinfected with VSVΔG-CC4XL (denoted by *, $p < 0.05$ and **, $p < 0.01$). (C) Aliquots of the supernatant fluids obtained on days 0, 1, and 3 post-VSV infection were serially diluted threefold and added to the Molt-4/OX40 cells cultured in the microtiter plates. Five days later, the plates were scored for the presence of EGFP$^+$ cells by fluorescence microscopy using the Olympus CKX41 microscope. The titers at each time point were determined by end-point titration and are displayed as IU/ml calculated. The data shown are representative of one of three similar independent experiments.

that do not express the HIV-1 Env at the cell surface of the Molt-4/IIIB/OX40 cells which are latently infected with HIV-1, and thus VSVΔG-CC4 was not able to eliminate the target cells completely. Such latently infected cells could however be easily targeted by the VSVΔG-CC4XL construct, as it does not need to bind the Env but can bind OX40 on the cell surface via its expression of OX40L. Given the fact that stimulation of OX40 with its cognate ligand induces HIV-1 production in the latently infected cells, followed by apoptotic cell death [21], the OX40-OX40L interaction might similarly activate the potentially latently infected cells among Molt-4/IIIB/OX40 cells and lead these cells to apoptosis. Otherwise HIV-1 production by the activation of the potentially latently infected cells might induce the expression of Env at the cell surface, leading to rVSV re-targeting/infection/killing of the cells.

Thus, the functional OX40L molecule expressed by VSVΔG-CC4XL appears to exert versatile effects upon superinfection that include virus–cell adhesion, cell activation and apoptotic cell death through the ligation with its receptor.

In an effort to further delineate the therapeutic window for such an approach, the duration of the antiviral effect of the rVSVs was

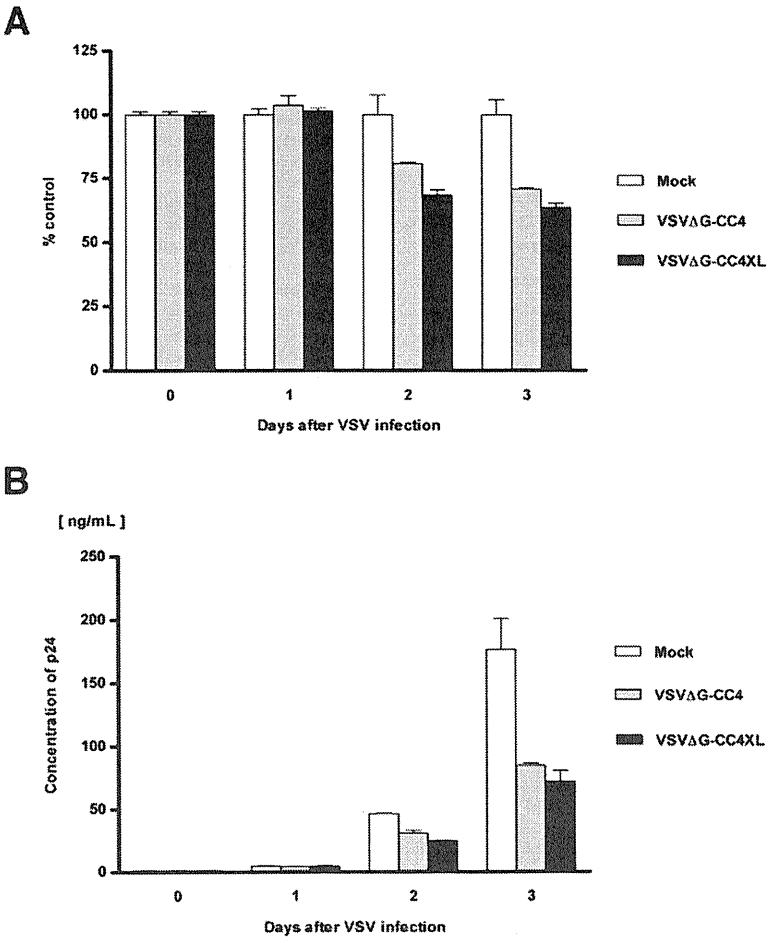

Fig. 6. Therapeutic potential of the rVSVs on activated primary CD4$^+$ T cells acutely infected with HIV-1. Primary CD4$^+$ T cells isolated were initially anti-CD3/CD28 stimulated for 3 days and then infected for 2 days with the recombinant X4 HIV-1 encoding EGFP. Aliquots of such infected cells were mock-infected or superinfected with either VSVΔG-CC4 or VSVΔG-CC4XL. The co-infected duplicate cultures were incubated for an additional 3 days. Each culture was harvested daily and the cells and supernatant fluid assayed. (A) The frequency of EGFP$^+$ (HIV-1–infected) cells was analyzed by flow cytometry daily after VSV infection. The results shown represent percentage of control values (mean + SE). (B) Aliquots of the supernatant fluids obtained were assayed daily by ELISA to determine levels of HIV-1 p24. The results shown represent percentage of control values (mean + SE). data displayed are representative of one of three similar independent experiments.

intriguing. As there was rapid and marked reduction in the number of Molt-4/IIIB/OX40 cells (Fig. 4B), we dispensed fresh Molt-4/IIIB/OX40 cells without the rVSVs directly into each culture three times during the experiment (for 10 days). It was of note that the progeny rVSVs in such cultures could keep killing the freshly added cells rapidly to the same extent as the initial cells placed in culture, indicating that these rVSVs retain their potential for a substantial time period. These data also suggest that OX40L as well as the HIV-1 receptors are consistently expressed on the progeny virions from the genome of replication-competent rVSV and stably expressed in a functional form sufficient enough to elicit effects through binding to their receptor/ligand even after a single administration of the rVSV.

However, it is important to note that the OX40 protein expressed by the HIV-1–infected cells becomes downregulated after the return of the cells from the activated to a resting state. Consequently, because the rVSVs primarily target HIV-1–infected activated T cells, the resting HIV-1–infected cells would have reduced susceptibility to elimination by the rVSVs. In this respect, the persistently/latently HIV-1–infected cell reservoirs that are resistant to HAART drugs would similarly be resistant to VSVΔG-CC4XL-induced cytolysis due to the decreased expression of OX40. Thus, other strategies need to be used to eliminate such latently infected cells.

Our anti–HIV-1 strategy has major potential advantages over HAART-based therapy because of the following reasons. (i) The rVSV specifically infects cells that are already HIV-(1) infected via the membrane fusion following receptor-Env binding and then kills the superinfected cells. Thus, such effector mechanisms are reasoned to more efficiently and rapidly target and eliminate HIV-1–producing cells. It is also reasonable to assume that such effector mechanisms would also target the HIV-1 latently infected cells once they are reactivated presumably using histone deacetylase inhibitors currently being planned for use in the clinic. (ii) Based on the fact that the rVSV is replication competent, it is expected to retain the therapeutic potential all during infection, as described above. Thus a novel therapy with intermittent, but not continuous, administrations of the rVSV might be possible. (iii) The rVSV only proliferates in HIV-1–infected cells and thus the levels of rVSV replication would be dependent on HIV-1 replication. Therefore, the rVSV infection would decline along with HIV-1 clearance, at least partially indicating relative safety in the use of rVSV. Minimally, it seems reasonable to suggest that the strategy advanced herein would be a powerful adjunct to HAART and in particular, other therapies aimed at reactivation of latently infected cells.

In summary, our findings obtained in the present studies demonstrate that the additional expression of OX40L by the rVSVΔG construct that also expresses the X4 HIV-1 receptors rendered the recombinant even more infectious and cytopathic for HIV-1–infected OX40$^+$ cells and has a relatively potent effect on HIV-1 infection in culture. These results indicate the usefulness of the

OX40 protein as a therapeutic target and underscore the high potential of VSVΔG-CC4XL as a novel drug.

Acknowledgments

We thank Dr J.K. Rose for generously providing the expression plasmids regarding VSV and BHK-G cells, and for his suggestive comments on the manuscript. We are also grateful to Dr Y. Koyanagi for kindly providing the expression plasmid for HIV-1 NL-EGFP strain and to Drs D.S. Lyles, M.A. Whitt, Y. Matsuura and H. Tani for generously providing the anti-VSV N mAb. We are further thankful to Dr A.A. Ansari for his helpful suggestions for the manuscript and to K. Fukagawa, T. Koma and S. Tateishi for their helpful assistance with the experiments.

This work was supported in part by Health and Labour Science Research Grant (Research on Publicly Essential Drugs and Medical Devices) from the Ministry of Health, Labour and Welfare of Japan; and Grant-in-Aid for Scientific Research (C) from Japan Society for the Promotion of Science.

Appendix. Supplementary data

Supplementary data associated with this article can be found, in the online version, at doi:10.1016/j.humimm.2011.01.007.

References

[1] Egger M, May M, Chene G, Phillips AN, Ledergerber B, Dabis F, et al. Prognosis of HIV-1-infected patients starting highly active antiretroviral therapy: A collaborative analysis of prospective studies. Lancet 2002;360:119–29.
[2] Yeni PG, Hammer SM, Hirsch MS, Saag MS, Schechter M, Carpenter C. et al. Treatment for adult HIV infection: 2004 Recommendations of the International AIDS Society-USA Panel. JAMA 2004;292:251–65.
[3] Berger EA, Moss B, Pastan I. Reconsidering targeted toxins to eliminate HIV infection: You gotta have HAART. Proc Natl Acad Sci U S A 1998;95:11511–3.
[4] Pincus SH, Fang H, Wilkinson RA, Marcotte TK, Robinson JE, Olson WC. In vivo efficacy of anti-glycoprotein 41, but not anti-glycoprotein 120, immunotoxins in a mouse model of HIV infection. J Immunol 2003;170:2236–41.
[5] Saavedra-Lozano J, Cao Y, Callison J, Sarode R, Sodora D. Jet E, et al. An anti-CD45RO immunotoxin kills HIV-latently infected cells from individuals on HAART with little effect on CD8 memory. Proc Natl Acad Sci U S A 2004;101:2494–9.
[6] Schnell MJ, Johnson JE, Buonocore L, Rose JK. Construction of a novel virus that targets HIV-1-infected cells and controls HIV-1 infection. Cell 1997;90:849–57.
[7] Mebatsion T, Finke S, Weiland F, Conzelmann KK. A CXCR4/CD4 pseudotype rhabdovirus that selectively infects HIV-1 envelope protein-expressing cells. Cell 1997;90:841–7.
[8] Somia NV, Miyoshi H, Schmitt MJ, Verma IM. Retroviral vector targeting to human immunodeficiency virus type 1-infected cells by receptor pseudotyping. J Virol 2000;74:4420–4.
[9] Gupta N, Arthos J, Khazanie P, Steenbeke TD, Censoplano NM, Chung EA, et al. Targeted lysis of HIV-infected cells by natural killer cells armed and triggered by a recombinant immunoglobulin fusion protein: Implications for immunotherapy. Virology 2005;332:491–7.
[10] Mallett S, Fossum S, Barclay AN. Characterization of the MRC OX40 antigen of activated CD4 positive T lymphocytes—a molecule related to nerve growth factor receptor. EMBO J 1990;9:1063–8.
[11] Latza U, Durkop H, Schnittger S, Ringeling J, Eitelbach F, Hummel M, et al. The human OX40 homolog: cDNA structure, expression and chromosomal assignment of the ACT35 antigen. Eur J Immunol 1994;24:677–83.
[12] Baker SJ, Reddy EP. Modulation of life and death by the TNF receptor superfamily. Oncogene 1998;17:3261–70.
[13] Tanaka Y, Inoi T, Tozawa H, Yamamoto N, Hinuma Y. A glycoprotein antigen detected with new monoclonal antibodies on the surface of human lymphocytes infected with human T-cell leukemia virus type-I (HTLV-I). Int J Cancer 1985;36:549–55.
[14] Miura S, Ohtani K, Numata N, Niki M, Ohbo K, Ina Y, et al. Molecular cloning and characterization of a novel glycoprotein, gp34, that is specifically induced by the human T-cell leukemia virus type I transactivator p40tax. Mol Cell Biol 1991;11:1313–25.
[15] Ohshima Y, Tanaka Y, Tozawa H, Takahashi Y, Maliszewski C, Delespesse G. Expression and function of OX40 ligand on human dendritic cells. J Immunol 1997;159:3838–48.
[16] Kondo K, Okuma K, Tanaka R, Zhang LF, Kodama A. Takahashi Y, et al. Requirements for the functional expression of OX40 ligand on human activated CD4+ and $CD8^+$ T cells. Hum Immunol 2007;68:563–71.
[17] Kondo K, Okuma K, Tanaka R, Matsuzaki G, Ansari AA, Tanaka Y. Rapid induction of OX40 ligand on primary T cells activated under DNA-damaging conditions. Hum Immunol 2008;69:533–42.
[18] Imura A, Hori T, Imada K, Kawamata S, Tanaka Y, Imamura S, et al. OX40 expressed on fresh leukemic cells from adult T-cell leukemia patients mediates cell adhesion to vascular endothelial cells: Implication for the possible involvement of OX40 in leukemic cell infiltration. Blood 1997;89:2951–8.
[19] Brocker T, Gulbranson-Judge A, Flynn S, Riedinger M, Raykundalia C, Lane P. CD4 T cell traffic control: In vivo evidence that ligation of OX40 on CD4 T cells by OX40-ligand expressed on dendritic cells leads to the accumulation of CD4 T cells in B follicles. Eur J Immunol 1999;29:1610–6.
[20] Gruss HJ, Dower SK. Tumor necrosis factor ligand superfamily: Involvement in the pathology of malignant lymphomas. Blood 1995;85:3378–404.
[21] Takahashi Y, Tanaka Y, Yamashita A, Koyanagi Y, Nakamura M, Yamamoto N. OX40 stimulation by gp34/OX40 ligand enhances productive human immunodeficiency virus type 1 infection. J Virol 2001;75:6748–57.
[22] Takahashi Y, Tanaka R, Yamamoto N, Tanaka Y. Enhancement of OX40-induced apoptosis by TNF coactivation in OX40-expressing T cell lines in vitro leading to decreased targets for HIV type 1 production. AIDS Res Hum Retrovir 2008;24:423–35.
[23] Shockett P, Difilippantonio M, Hellman N, Schatz DG. A modified tetracycline-regulated system provides autoregulatory, inducible gene expression in cultured cells and transgenic mice. Proc Natl Acad Sci U S A 1995;92:6522–6.
[24] Miura Y, Misawa N, Maeda N, Inagaki Y, Tanaka Y, Ito M, et al. Critical contribution of tumor necrosis factor-related apoptosis-inducing ligand (TRAIL) to apoptosis of human $CD4^+$ T cells in HIV-1-infected hu-PBL-NOD-SCID mice. J Exp Med 2001;193:651–60.
[25] Lawson ND, Stillman EA, Whitt MA, Rose JK. Recombinant vesicular stomatitis viruses from DNA. Proc Natl Acad Sci U S A 1995;92:4477–81.
[26] Schnell MJ, Buonocore L, Whitt MA, Rose JK. The minimal conserved transcription stop-start signal promotes stable expression of a foreign gene in vesicular stomatitis virus. J Virol 1996;70:2318–23.
[27] Fuerst TR, Niles EG, Studier FW, Moss B. Eukaryotic transient-expression system based on recombinant vaccinia virus that synthesizes bacteriophage T7 RNA polymerase. Proc Natl Acad Sci U S A 1986;83:8122–6.
[28] Roberts A, Buonocore L, Price R, Forman J, Rose JK. Attenuated vesicular stomatitis viruses as vaccine vectors. J Virol 1999;73:3723–32.
[29] Page KA, Landau NR, Littman DR. Construction and use of a human immunodeficiency virus vector for analysis of virus infectivity. J Virol 1990;64:5270–6.
[30] Sutton RE, Littman DR. Broad host range of human T-cell leukemia virus type 1 demonstrated with an improved pseudotyping system. J Virol 1996;70:7322–6.
[31] Okuma K, Boritz E, Walker J, Sarkar A, Alexander L, Rose JK. Recombinant vesicular stomatitis viruses encoding simian immunodeficiency virus receptors target infected cells and control infection. Virology 2006;346:86–97.

AIDS-2011-0073-ver9-Nakayama_1P
Type: research-article

AIDS RESEARCH AND HUMAN RETROVIRUSES
Volume 27, Number 00, 2011

DOI: 10.1089/aid.2011.0073

Imbalanced Production of Cytokines by T Cells Associates with the Activation/Exhaustion Status of Memory T Cells in Chronic HIV Type 1 Infection

Kaori Nakayama,[1] Hitomi Nakamura,[2] Michiko Koga,[2] Tomohiko Koibuchi,[2] Takeshi Fujii,[2] Toshiyuki Miura,[1] Aikichi Iwamoto,[1,2] and Ai Kawana-Tachikawa[1]

Abstract

Chronic HIV-1 infection is characterized by immune cell dysfunctions driven by chronic immune activation. Plasma HIV-1 viral load (VL) is closely correlated with disease progression and the level of immune activation. However, the mechanism by which the persistent presence of HIV-1 damages immune cells is still not fully understood. To evaluate how HIV-1 affects disruption of T cell-mediated immune responses during chronic HIV-1 infection we determined the functional profiles of T cells from subjects with chronic HIV-1 infection. We measured the capacity of peripheral blood mononuclear cells (PBMCs) to produce 25 specific cytokines in response to nonspecific T cell stimulation, and found that the capacity to produce Th-1-related cytokines (MIP-1α, MIP-1β, RANTES, IFN-γ, and MIG), sIL-2R, and IL-17, but not Th-2-related cytokines, was inversely correlated with plasma VL. The capacities to produce these cytokines were interrelated; notably, IL-17 production had a strong direct correlation with production of MIP-1α, MIP-1β, RANTES, and IFN-γ. In both $CD4^+$ and $CD8^+$ T cells, dysfunctional production of cytokines was associated with T cell activation (CD38 expression) and exhaustion (PD-1 and/or CTLA-4 expression) status of memory subsets. Although the capacity to produce these cytokines was recovered soon after multiple $\log_{10}$ reduction of plasma viral levels by antiretroviral therapy, memory $CD8^+$ T cells remained activated and exhausted after prolonged virus suppression. Our data suggest that HIV-1 levels directly affect the ability of memory T cells to produce specifically Th1- and Th17-related cytokines during chronic HIV-1 infection.

Introduction

PLASMA VIRAL LOAD (VL) and CD4-positive T cell count are two surrogate markers of HIV-1 disease progression.[1] Throughout the course of infection both innate and adaptive immune systems are highly activated, and disease progression is strongly correlated with immune activation status.[2,3] Notably, immune activation is observed in both HIV-1 and pathogenic SIV infection, but not in nonpathogenic SIV infection in a natural host.[4,5] Moreover, studies have shown that T cells in patients with high VL and progressive disease are less functional, have less proliferative capacity, and are more exhausted than T cells in patients with low VL and slow disease progression.[6–12] In those patients, exhaustion is seen not only in HIV-1-specific T cells, but also in nonspecific T cells.[11,13] These data suggest that immune cells have lost their original function due to persistent hyperactivation, which depends on VL, during chronic HIV-1 infection.

The immune system is highly coordinated: the cytokine network regulates interactions between cells, and cytokine balance dictates how the immune system responds. Cytokine production determines the specific helper functions of $CD4^+$ T cells and allows balance in immune responses *in vivo*.[14–16] A possible explanation of the impaired immune response in chronic HIV-1 infection is that the ability of T cells to balance cytokine production has been altered, just as alteration of balance between Th1- and Th2-type immune response affects the clinical course of certain infectious diseases and autoimmune syndromes.[17,18]

To evaluate T cell impairment resulting from persistent immune activation during chronic HIV-1 infection, we compared the cytokine expression spectra of peripheral blood mononuclear cells (PBMCs) in response to nonspecific T cell stimulation in treatment-naive HIV-1-infected subjects with low or high VL. We also examined the differentiation states and activation levels of $CD4^+$ and $CD8^+$ T cells from

[1]Division of Infectious Diseases, Advanced Clinical Research Center, and [2]Department of Infectious Diseases and Applied Immunology, Research Hospital, The Institute of Medical Science, The University of Tokyo, Tokyo, Japan.

HIV-1-infected subjects to elucidate relationships between cytokine expression capacity and T cell phenotypic status.

Materials and Methods

Study design

HIV-1-infected individuals who were under medical supervision at our clinic were asked to provide blood samples for this study. Blood samples were taken from selected patients in the chronic phase of HIV-1 infection, with CD4 counts >200 cells/ml. We requested blood samples from antiretroviral therapy (ART)-naive patients with either low plasma viral load (VL) values (<5000 copies/ml; LVL group) or high VL values (>25,000 copies/ml; HVL group), and from treatment-experienced patients who had received ART >2 years (Tx group). Blood samples were also obtained from a small number of HIV-1-infected patients who had first initiated ART within the previous 1–2 months. As controls, blood samples were obtained from HIV-1-seronegative individuals (healthy controls; HC).

All participants gave written informed consent, and the study was approved by the institutional review boards of the Institute of the Medical Science of the University of Tokyo (No. 11-2-0329 and 20-47-210521).

PBMC cultures and PHA stimulation

PBMCs were isolated from heparinized whole blood by Ficoll-Paque PLUS density gradients (GE Healthcare, Piscataway, NJ) and cryopreserved in liquid nitrogen until use. The frozen cells were thawed 1 day before stimulation and cultured in R10 medium [RPMI 1640 medium (Sigma, St. Louis, MO) supplemented with 10% heat-inactivated fetal calf serum (FCS; Sigma), 100 U penicillin/ml, 100 μg/ml streptomycin (Sigma), 2 mmol/liter L-glutamine (Sigma), and 10 mmol/liter 4-(2-hydroxyethyl)-1-piperazineethanesulfonic acid (HEPES; Sigma)] at 37°C, 5% CO_2. The following day 5×10^5 cells/well were cultured in 250 μl/well of R10 medium with or without 2 μg/ml phytohemagglutinin L (PHA; Roche Applied Science, Mannheim, Germany). Culture supernatants were harvested after 48 h and stored at −80°C until use for multiple cytokine assays.

Quantification of cytokines

The human cytokine 25-plex antibody kit (Invitrogen Corporation, Carlsbad, CA) was used to measure the levels of 25 cytokines in culture supernatants: interleukin (IL)-1 receptor antagonist protein (IL-1RA), IL-1β, IL-2, soluble IL-2R (sIL-2R), IL-4, IL-5, IL-6, IL-7, IL-8, IL-10, IL-12p40/70, IL-13, IL-15, IL-17, eotaxin, interferon gamma (IFN-γ)-induced protein 10 kDa (IP-10), monocyte chemoattractant protein-1 (MCP-1), monokine induced by IFN-γ (MIG), macrophage inflammatory protein 1alpha (MIP-1α), MIP-1β, regulated on activation normal T cell expressed and secreted (RANTES), tumor necrosis factor-α (TNF-α), granulocyte-macrophage colony-stimulating factor (GM-CSF), IFN-α, and IFN-γ. The detection limits for the cytokines measured by the kit were as follows: IL-5, IL-6, IL-8, 3 pg/ml; MIG, 4 pg/ml; IL-4, IL-10, IFN-γ, IP-10, eotaxin, 5 pg/ml; IL-2, 6 pg/ml; IL-7, IL-13, IL-15, IL-17, TNF-α, MIP-1α, MIP-1β, MCP-1, 10 pg/ml; IL-1β, IL-12p40/70, IFN-α, GM-CSF, RANTES, 15 pg/ml; IL-1RA, sIL-2R, 30 pg/ml. As the amounts of IL-6, IL-8, TNF-α, MIP-1α, MIP-1β, IP-10, MIG, and MCP-1 produced from PHA-stimulated PBMCs were beyond the range of the assay, we diluted the samples 10-fold prior to measurement of these cytokines. However, IL-8 levels were out of range in most patient samples and could not be measured accurately.

Samples were loaded onto the Luminex100 system (Luminex Corporation, Austin, YX), and samples were quantified by analysis of the median fluorescence intensity of the beads using MasterPlex QT version 2.5 (Luminex Corporation). The assays were performed according to the manufacturer's instructions, and all samples were run in duplicate.

Identification of cytokine-producing cells in PBMCs

$CD14^+$ cells (monocytes), $CD8^+$ T cells, $CD4^+$ T cells, and $CD56^+CD16^+$ (NK) cells were isolated sequentially from PBMCs of each healthy subject. Magnetic cell separation (MACS) selection was performed using anti-CD14, anti-CD8, and anti-CD4 antibody-conjugated microbeads or using the $CD56^+CD16^+$ NK cell isolation kit (Miltenyi Biotic, Bergisch Gladbach, Germany). The purity of each cell fraction was >95% as determined by flow cytometry.

Fractionated cells were cultured separately or were co-cultured in the presence of 2 μg/ml PHA at 37°C, 5% CO_2, for 48 h. Levels of MIP-1α, MIP-1β, RANTES, IL-2R, IFN-γ, and IL-17 in culture supernatants were measured with DuoSet ELISA Development Systems (R&D Systems). The absolute numbers of each cell fraction used in the experiments were calculated from the average proportion of each subset in PBMCs.

Antibodies

The fluorochrome-conjugated monoclonal antibodies (mAb) used in the study were as follows: fluorescein isothiocyanate (FITC)-labeled anti-MIP-1α, anti-MIP-1β, and anti-RANTES (R&D Systems, Minneapolis, MN); FITC-labeled anti-PD-1 and anti-Ki67, phycoerythrin (PE)-labeled anti-Bcl-2, peridinin cholorophyll protein/cyanin5.5 (PerCP Cy5.5)-labeled anti-CD38 and anti-CD3, PE Cy7-labeled anti-CCR7, allophycocyanin (APC)-labeled anti-CD45RA, and pacific blue-labeled anti-CD4 (BD Biosciences, San Jose, CA); APC AlexaFluor 750-labeled anti-CD4, pacific blue-labeled anti-IFN-γ, and AlexaFluor 647-labeled anti-IL-17A (eBioscience, San Diego, CA); PE-labeled anti-IL-4 (Becton Dickinson, Franklin Lakes, NJ); APC Cy7-labeled anti-CD3 (BioLegend, San Diego, CA); and Pacific Orange-labeled anti-CD8 (Invitrogen).

Surface phenotypic and intracellular cytokine staining

For intracellular cytokine staining, cryopreserved PBMCs were thawed and cultured in R10 overnight. The following day cells were stimulated with phorbol ester (PMA)/calcium ionophore (ionomycin) in the presence of Golgi inhibitor (brefeldin A) for 5 h. Cells were stained with a panel of fluorescently labeled antibodies against cell-surface markers. For detection of dead cells, the cells were also stained with 5 μg/ml ethidium monoazide bromide (EMA; Sigma). Cells were washed twice and exposed to fluorescent light for 10 min on ice to allow the EMA to bind to DNA in dead cells. Cells were then fixed in 2% paraformaldehyde and permeabilized in BD FACS Permeabilizing Solution 2 (BD Biosciences) prior to antibody staining for intracellular molecules.

Dead or dying cells were detected by surface phenotypic staining with propidium iodide (PI; Sigma).

Flow cytometric analysis

Samples were analyzed on a FACSAria multilaser cytometer (Beckton Dickinson) running FACSDiva software, with collections of 60,000–100,000 lymphocyte-gated events. Data were analyzed with FlowJo software (Tree Star, Ashland, OR).

Statistical analysis

GraphPad Prism5 software (San Diego, CA) was used for all statistical analysis. Differences between groups were tested for statistical significance using the nonparametric Mann–Whitney *U* test. Since previous studies revealed that production of multiple cytokines by HIV-specific T cells was limited in progressors compared to nonprogressors,[6,19] the production levels of cytokines were expected to differ among LVL, HVL, and healthy control subjects. For this reason, we did not consider multiple comparison correction for Mann–Whitney *U* tests to avoid false-negative results. Correlation analysis was performed using Spearman's rank correlation. The level of significance for all analyses was set at $p < 0.05$.

Results

Study population

Most analyses were performed using blood samples collected from 35 HIV-1-infected, ART-naïve patients, 15 HIV-1-infected, treatment-experienced patients, and 16 HIV-1-seronegative individuals. Demographic characteristics of these 50 HIV-1-infected patients are presented in Table 1. The 35 HIV-1-infected, ART-naive patients included 19 patients with low VL (LVL group; median VL: 1200, range: 53 to 3600) and 16 patients with high VL (HVL group; median VL: 62,000; range: 25,000 to 500,000). The median CD4 counts in the LVL and HVL groups were 449 (range: 316 to 749) and 407 (range: 228 to 520), respectively; the difference was not statistically significant. The groups also showed no significant difference in age, another factor that influences immune status.

The 15 HIV-1-infected individuals recruited into the study to represent treatment-experienced patients had received ART and successfully controlled their disease over a long period of time (median: 66 months; range: 22 to 149 months). To examine the impact of actively decreasing VL on the functional profile of PBMCs, blood samples were also collected from six HIV-1-infected patients who had initiated treatment only in the previous 1–2 months.

Cytokine production in PHA-stimulated PBMCs

Cytokine measurements from cells cultured for 48 h in an unstimulated state were at the limit of detection (data not shown). We initially compared anti-CD3-antibody and PHA as a nonspecific stimulus of PBMCs to induce cytokine production, and found that the production levels of most cytokines were much higher in PHA-stimulated PBMCs than in anti-CD3-antibody-stimulated PBMCs (data not shown). When cells were stimulated with PHA and cultured for 48 h, production of most cytokines increased dramatically (Fig. 1A). There were no significant differences between any groups in IL-2, IL-13, IL-15, IL-1β, IFN-α, TNF-α, eotaxin, or IP-10 production (data not shown).

Cytokine production in PBMCs from treatment-naive HIV-1 subjects was compared to cytokine production in PBMCs from healthy control subjects. Median levels of many cytokines in the HVL group were significantly different from those in the healthy control group: MIP-1α [6.33 (range 0.99–21.01) vs. 16.92 (10.36–23.87) ng/ml; $p = 0.0005$], MIP-1β [8.51 (1.37–26.42) vs. 21.44 (10.26–34.11) ng/ml; $p = 0.0036$], IFN-γ [1.50 (0.30–5.75) vs. 2.64 (0.79–5.78) ng/ml; $p = 0.0402$], IL-7 [<0.01 (<0.01–0.67) vs. 0.04 (<0.01–0.07) ng/ml; $p = 0.0077$], IL-1Ra [18.93 (0.59–27.61) vs. 1.50 (0.55–14.95) ng/ml; $p = 0.0184$], IL-6 [0.63 (0.11–12.23) vs. 1.77 (0.68–4.93) ng/ml; $p = 0.0254$], and IL-10 [0.08 (<0.005–0.40) vs. 0.55 (0.13–0.83) ng/ml; $p = 0.0031$]. In contrast, significant differences between the LVL group and the healthy control group were seen only in levels of IL-10 [0.12 (<0.005–0.72) vs. 0.55 (0.13–0.83) ng/ml; $p = 0.0050$] and IL-1Ra [17.05 (0.49–28.31) vs. 1.50 (0.55–14.95) ng/ml; $p = 0.0282$] (Fig. 1A). These data suggest that although PBMCs from HVL subjects are abnormal in some way, PBMCs from LVL subjects are almost normal in terms of cytokine production.

As shown in Fig. 1A, mean cytokine levels were significantly lower in HVL subjects compared to LVL subjects, as follows: MIP-1α [6.33 (0.99-21.01) vs. 14.36 (2.29–29.16) ng/ml; $p = 0.0077$], MIP-1β [8.51 (1.37–26.42) vs. 20.14 (4.31–48.75) ng/ml; $p = 0.0034$], RANTES [2.01 (<0.015–4.57) vs. 3.40 (1.33–6.90) ng/ml; $p = 0.0014$], sIL-2R [2.30 (0.02–4.96) vs. 3.72 (1.72–7.38) ng/ml; $p = 0.0136$], IL-17 [0.04 (<0.01–0.12) vs. 0.08 (<0.01–0.17) pg/ml; $p = 0.0256$], and IL-7 [<0.01 (<0.01–0.67) vs. 0.05 (<0.01–1.05) pg/ml; $p = 0.0029$]. Notably, there was an inverse correlation between VL and production of these cytokines, and of IFN-γ (Fig. 1B). No relationship was observed between cytokine levels and CD4 cell count (data not shown). These data suggest that VL directly affects the capacity of PBMCs to produce certain cytokines during chronic infection.

Th1- and Th17-type T cells have impaired cytokine production in HVL subjects

Although PHA is considered a T cell mitogen, other cell populations also produce cytokines in response to PHA stimulation.[20–22] The next step was to determine which cells were responsible for the alterations in cytokine production observed under our experimental conditions. The cytokines whose production was inversely correlated with VL can be produced by several cell populations in PBMCs. To identify the major cell population producing these cytokines, we fractionated PBMCs in healthy donors by positive selection and determined the cell population producing these cytokines. $CD4^+$ T cells, $CD8^+$ T cells, monocytes ($CD14^+$), and NK cells ($CD56^+CD16^+$) were isolated from PBMCs, cultured separately or cocultured, and stimulated with PHA. We then measured levels of MIP-1α, MIP-1β, RANTES, IFN-γ, sIL-2R, and IL-17. Little or no production of these cytokines was detected in any of the single cell fractions (Fig. 2A). Production of cytokines MIP-1α, MIP-1β, RANTES, IFN-γ, and sIL-2R was observed in cocultures of $CD4^+$ and $CD14^+$ cells and in cocultures of $CD8^+$ and $CD14^+$ cells (Fig. 2A, and data not shown). IL-17 production was detected only in cocultures of $CD4^+$ and $CD14^+$ cells (Fig. 2A). As T cell stimulation by